

JGR Space Physics



RESEARCH ARTICLE

10.1029/2023JA032193

Key Points:

- A method for inferring equatorial wave power gain from low altitude electron flux measurements based on quasilinear theory is described
- The inferred chorus wave power gain increases roughly linearly with equatorial 180–300 keV trapped electron flux during moderate storms
- Inferred chorus wave power gains typically reach 10 near the upper flux limit

Correspondence to:

D. Mourenas, didier.mourenas@cea.fr

Citation:

Mourenas, D., Artemyev, A. V., Zhang, X.-J., & Angelopoulos, V. (2024). Checking key assumptions of the Kennel-Petschek flux limit with ELFIN CubeSats. *Journal of Geophysical Research: Space Physics*, 129, e20231A032193. https://doi.org/10.1029/2023JA032193

Received 17 OCT 2023 Accepted 28 JAN 2024

©2024. The Authors. This is an open access article under the terms of the Creative Commons Attribution License, which permits use, distribution and reproduction in any medium, provided the original work is properly cited.

Checking Key Assumptions of the Kennel-Petschek Flux Limit With ELFIN CubeSats

D. Mourenas^{1,2}, A. V. Artemyev³, X.-J. Zhang^{3,4}, and V. Angelopoulos³

¹CEA, DAM, DIF, Arpajon, France, ²Laboratoire Matière en Conditions Extrêmes, Paris-Saclay University, CEA, Paris, France, ³Department of Earth, Planetary, and Space Sciences, University of California, Los Angeles, CA, USA, ⁴Department of Physics, University of Texas at Dallas, Richardson, TX, USA

Abstract In planetary radiation belts, the Kennel-Petschek flux limit is expected to set an upper limit on trapped electron fluxes at 80-600 keV in the presence of efficient electron loss through pitch-angle diffusion by whistler-mode chorus waves generated around the magnetic equator by the same 80-600 keV electron population. Comparisons with maximum measured fluxes have been relatively successful, but several key assumptions of the Kennel-Petschek model have not been experimentally tested. The Kennel-Petschek model notably assumes an exponential growth of chorus waves as the trapped electron flux increases, and a fixed maximum wave power gain of about 3. Here, we describe a method for inferring the near-equatorial wave power gain using only measurements of trapped, precipitating, and backscattered electron fluxes at low altitude. Next, we make use of Electron Losses and Fields Investigation (ELFIN) CubeSats measurements of such electron fluxes during two moderate geomagnetic storms with sustained electron injections to infer the corresponding chorus wave power gains as a function of time, energy, and equatorial trapped electron flux. We show that wave power increases exponentially with trapped flux, with a wave power gain roughly proportional to the theoretical linear convective gain, and that the maximum inferred gain near the upper flux limit is roughly 10, with a factor of 2 uncertainty. Therefore, two key theoretical underpinnings of the Kennel-Petschek model are borne out by the present results, although the strong inferred gains should correspond to higher flux limits than in traditional estimates.

1. Introduction

Resonant interactions between whistler-mode chorus waves and electrons are known to play an important role in the dynamics of electron fluxes in the radiation belts of the Earth and of other planets (e.g., see Thorne et al., 2013; W. Li & Hudson, 2019). Prolonged disturbed periods during geomagnetic storms or successive substorms frequently lead to the formation of a growing peak of MeV electron phase space density (PSD) at $L \simeq 4.5 - 5.5$ outside the plasmasphere of the Earth, suggesting a key role of chorus wave driven electron acceleration in producing such localized peaks (Boyd et al., 2018; Hua, Bortnik, & Ma, 2022; Tang et al., 2017; Turner et al., 2013).

Chorus waves are excited near the magnetic equator during geomagnetic storms and substorms by unstable populations of energetic electrons injected from the plasma sheet (Tsurutani & Smith, 1974; W. Li et al., 2010; Tao et al., 2011). Nonlinear chorus wave growth takes over above some threshold wave amplitude allowing electron trapping and leads to the formation of intense quasi-parallel lower-band (between 1/10 and 1/2 of the electron gyrofrequency Ω_{ce}) chorus elements with characteristic rising tones during their propagation from the magnetic equator to higher latitudes (Demekhov, 2011; Demekhov & Trakhtengerts, 2008; Nogi & Omura, 2023; Nunn et al., 2009; Omura, 2021; Omura et al., 2008; Tao et al., 2020). Each nonlinearly growing rising tone chorus element consists of several wave packets (often called "subpackets" in this case), and the amplitude of each wave packet is theoretically limited by the optimum wave amplitude maximizing nonlinear wave growth, although this optimum/maximum wave amplitude is not the same for each wave packet (Katoh et al., 2018; Omura & Nunn, 2011).

Spacecraft observations and numerical simulations show that different chorus waves, excited at the same or different times and locations with different frequencies and wave-normal angles, are often superposed, leading to the ubiquitous formation of short wave packets characterized by important and random wave frequency and phase jumps between (but also within) packets and relatively moderate peak amplitudes $\sim 100-200$ pT (Mourenas, Zhang, et al., 2022; Zhang, Agapitov, et al., 2020; Zhang et al., 2021; Zhang, Mourenas, et al., 2020). Since such

MOURENAS ET AL. 1 of 21

superposed chorus waves usually nearly satisfy the Chirikov criterion for resonance overlap (Mourenas, Zhang, et al., 2022; Shapiro & Sagdeev, 1997), a further growth of their amplitude would lead to resonance overlap and a stochastization of electron motion, quenching their nonlinear growth (Mourenas, Zhang, et al., 2022), especially in the presence of an increasing geomagnetic field inhomogeneity toward higher latitudes that increases the stochastization of electron motion (Albert, 1993, 2001; Shklyar, 1981; Solovev & Shkliar, 1986). As a result, resonant interactions between trapped electrons and short chorus wave packets usually remain in a regime close to quasi-linear diffusion (Allanson et al., 2020; An et al., 2022; Artemyev, Mourenas, et al., 2022; Gan et al., 2022; Mourenas, Zhang, et al., 2022; Zhang, Agapitov, et al., 2020).

The Kennel-Petschek flux limit is expected to be imposed by a net loss of trapped electrons through precipitation into the atmosphere via quasi-linear pitch-angle diffusion by whistler-mode waves generated by the same electron population (Kennel & Petschek, 1966; Summers et al., 2009). The linear growth rate of chorus waves is proportional to the flux J_{trap} of trapped electrons in cyclotron resonance with the waves at high equatorial pitchangles (Kennel & Petschek, 1966; Mourenas, Zhang, et al., 2022; Summers et al., 2009; Tao et al., 2017) and the nonlinear growth rate can be $\approx 2-10$ times larger than the linear growth rate (Shklyar & Matsumoto, 2009; Summers et al., 2011, 2013). The convective wave power gain $G = \gamma \Delta s/v_o$ is proportional to the linear (and nonlinear) growth rate γ , to the distance Δs of wave growth along a magnetic field line, and inversely proportional to the wave parallel group velocity v_g (Summers et al., 2009). Accordingly, the Kennel-Petschek flux limit assumes the generation of waves of exponentially higher magnetic wave power $B_w^2/B_{w,KP}^2 \simeq \exp[G(J_{trap})]$ $-G_0] \simeq \exp\left[\left(J_{trap}/J_{KP}-1\right)G_0\right]$ as the trapped electron flux J_{trap} increases above the Kennel-Petschek flux limit J_{KP} (which corresponds to a gain G_0 and a wave power $B^2_{w,KP}$), leading in the weak diffusion regime to exponentially faster electron loss and preventing a significant increase of J_{trap} above J_{KP} (Kennel & Petschek, 1966). A fixed wave power gain $G(J_{trap} = J_{KP}) = G_0 = 3$ at the Kennel-Petschek limit is deemed sufficient for the needed fast electron loss (Kennel & Petschek, 1966; Summers et al., 2009). Summers et al. (2009) assumed a fixed linear gain $G_0 = 3$ over $\Delta s = LR_E/2$ (with R_E the Earth's radius), equivalent to a total linear and nonlinear gain $G_0 = 3$ over $\Delta s \simeq LR_F/10 - LR_F/5$ consistent with the statistical increase of chorus wave power up to magnetic latitudes $\lambda \approx 6^{\circ} - 10^{\circ}$ at 4–14 MLT when Kp > 3 (Agapitov et al., 2018) and with theoretical estimates of the latitudinal extent of the chorus wave source region (Demekhov et al., 2003, 2017; Trakhtengerts

The Kennel-Petschek flux limit has been successfully compared with measured maximum fluxes of $\sim 100-300$ keV electrons in the Earth's outer radiation belt, as well as in other planetary radiation belts, and it has been widely used for predicting maximum electron fluxes in the radiation belts (Chakraborty et al., 2022; Kennel & Petschek, 1966; Mauk & Fox, 2010; Olifer et al., 2021, 2022; Schulz & Davidson, 1988; Summers et al., 2009; Summers & Shi, 2014). However, recent works have shown the existence of a second, different upper limit on trapped electron fluxes, due to a dynamical equilibrium in the presence of injections and both chorus wave-driven electron acceleration and loss, which is also in good agreement with measurements during strong injection events (Hua, Bortnik, & Ma, 2022; Mourenas, Artemyev, et al., 2022; Mourenas et al., 2023). This second upper limit may also correspond to a chorus wave power gain proportional to J_{trap} . But in this case, wave-driven electron acceleration (explicitly neglected in the Kennel-Petschek mechanism) can lead to an increase of electron flux up to a steady state and suppress, above $\sim 100-300$ keV, the net electron loss needed in the Kennel-Petschek flux limitation mechanism (Hua, Bortnik, & Ma, 2022; Mourenas, Artemyev, et al., 2022; Mourenas et al., 2023). This raises the possibility that the Kennel-Petschek flux limit might not always be relevant in the radiation belts.

To assess the actual role played by the Kennel-Petschek flux limit in determining maximum electron fluxes reached during strong and prolonged disturbances, it is therefore essential to check its main assumptions. In the present paper, we use the ELFIN dual CubeSat mission's (Angelopoulos et al., 2020, 2023) low-altitude measurements of trapped, precipitating, and backscattered electron fluxes at $\sim 80-600$ keV during geomagnetic storms, combined with quasi-linear diffusion theory, to check whether two key assumptions of the Kennel-Petschek model, namely, a fixed maximum chorus wave power gain $G_0 \simeq 3$ at the upper flux limit and an exponential increase of wave power with trapped flux J_{trap} , are valid in the outer radiation belt of the Earth. In Section 2, we first provide the detailed methodology and equations for inferring the chorus wave power gain as a function of time and trapped energetic $\sim 80-600$ keV electron flux based on low-altitude spacecraft measurements combined with quasi-linear theory in the weak diffusion regime. Next, this methodology is applied in

MOURENAS ET AL. 2 of 21



Section 3 to examine the validity of the above key assumptions of the Kennel-Petschek model during two moderate storms, and the results are discussed in Section 4.

2. Methodology for Inferring Wave Power Gain During Geomagnetic Storms and Substorms From Low-Altitude ELFIN CubeSat Data

2.1. Generalities

In the Earth's outer radiation belt at $L \sim 4.5 - 6.5$, whistler-mode lower-band chorus waves are excited near the magnetic equator by unstable anisotropic populations of energetic electrons injected from the plasma sheet (W. Li et al., 2010) and later grow non-linearly up to relatively large amplitudes (Nogi & Omura, 2023; Omura et al., 2008). In the present section, we provide a detailed method for determining the evolution of the chorus wave power gain G(t) during the course of a geomagnetic storm as a function of the trapped electron flux $J_{trap}(t)$, making use of low-altitude ELFIN CubeSat measurements of trapped, precipitating, and backscattered electron flux (Angelopoulos et al., 2020) combined with quasi-linear diffusion theory in the weak diffusion regime (Kennel & Petschek, 1966; Summers & Shi, 2014).

As will appear below, this method requires energy-resolved measurements of trapped electron fluxes J_{trap} at pitch-angles just above the loss cone (for ELFIN data, at $\alpha_0 \simeq 1.05~\alpha_{0,LC}$ where α_0 and $\alpha_{0,LC}$ denote the equatorial pitch-angle and loss cone angle, respectively), and energy-resolved data of both precipitating electron fluxes $J_{prec,meas}$ measured above ELFIN within the local bounce loss cone and backscattered (by the atmosphere) electron fluxes J_{up} measured below ELFIN within the local anti-loss-cone (see examples of measured trapped, precipitating and backscattered fluxes in Figure 1 from Mourenas et al., 2023), sufficiently well resolved in pitch-angle, to allow an accurate determination of the average (over local pitch-angles) effective net flux $J_{prec} \simeq J_{prec,meas} - J_{up}$ of electrons precipitated by whistler-mode waves within the loss cone (Mourenas et al., 2023). The low-altitude ELFIN CubeSats precisely provide the needed electron flux data with a good resolution in pitch-angle within the loss cone (Angelopoulos et al., 2020, 2023). An absence of measurements of backscattered electron flux or a too low pitch-angle resolution of the precipitating flux in the loss cone would significantly increase potential errors in the determination of the inferred wave power gains, even during active times (Mourenas et al., 2021).

2.2. Event Selection

First of all, we focus on moderate storms with a minimum Dst comprised between -49 and -65 nT at $L \simeq 4-6$, such as the 16-18 April 2021 storm. Such events with high time-integrated AE and ap indices (Hua, Bortnik, Chu, et al., 2022; Mourenas, Artemyev, et al., 2022; Mourenas et al., 2019) are characterized by strong injections of energetic $\sim 30-300$ keV electrons from the plasma sheet (Xiong et al., 2018), allowing strong chorus wave generation and chorus wave-driven electron acceleration and precipitation into the atmosphere (Horne et al., 2005; Omura et al., 2008; Summers et al., 1998; Thorne et al., 2013), often leading to an increase of $\sim 0.1-2$ MeV electron fluxes at $L \sim 5$ up to their highest recorded levels (Hua, Bortnik, Chu, et al., 2022; Hua, Bortnik, & Ma, 2022; Mourenas, Artemyev, et al., 2022; Mourenas et al., 2019; Mourenas et al., 2023). The maximum electron fluxes reached during these events with high time-integrated AE and ap indices are apparently close to an upper limit, from ~ 80 keV to ~ 2 MeV, set either by the Kennel-Petschek flux limit (Kennel & Petschek, 1966; Olifer et al., 2022; Summers et al., 2009; Summers & Shi, 2014) or by a dynamical equilibrium in the presence of injections and both chorus wave-driven energy and pitch-angle diffusion (Hua, Bortnik, & Ma, 2022; Mourenas, Artemyev, et al., 2022; Mourenas et al., 2023).

The present method applies only during active periods with strong and sustained injections, such that the trapped electron flux is steadily and significantly increasing, the precipitating flux J_{prec} is not too close to the instrument noise level (~100 e/cm²/s/sr/MeV), and J_{prec}/J_{trap} is not too low and also significantly increasing, to keep uncertainties on inferred wave power gain values within reasonable bounds. During quiet times without strong and sustained injections, the measured trapped electron flux just above the loss cone is not increasing, but decreasing with significant fluctuations in MLT and universal time, and J_{prec} is usually near the noise level and even more strongly fluctuating (e.g., see Mourenas et al., 2021), which would lead to very large uncertainties and fluctuations in estimated wave power gains. For instance, the presence or absence of only one intense chorus wave packet can affect much more strongly a small J_{prec}/J_{trap} ratio than the higher J_{prec}/J_{trap} ratios observed during active times. In addition, to investigate regions at $L \le 6$ and 4–14 MLT (see below) where the chorus wave power

MOURENAS ET AL. 3 of 21

latitudinal distribution is well known and weakly varying with geomagnetic activity (Agapitov et al., 2018), we must focus on active periods with AE > 150 nT or Kp > 1.6 during which such regions are located outside the plasmapause (Agapitov et al., 2019; O'Brien & Moldwin, 2003).

2.3. Analysis of Electron Fluxes

We exclude ELFIN measurements in the South Atlantic Anomaly sector and only examine electron energies $\sim 0.08-0.6$ MeV at times when there is no peak of the precipitating to trapped flux ratio $J_{prec}/J_{trap} > 0.5$ above 1 MeV, to exclude EMIC wave-driven precipitation (Angelopoulos et al., 2023). This energy range, $\sim 0.08-0.6$ MeV, corresponds to the main population of cyclotron resonant electrons with equatorial pitch-angles $\alpha_0 > 60^\circ$ efficiently generating parallel chorus waves of mean normalized frequency $\omega/\Omega_{ce0} \simeq 0.2-0.25$ (Agapitov et al., 2018; W. Li et al., 2016) for a typical plasma frequency to gyrofrequency ratio $\Omega_{pe0}/\Omega_{ce0} \simeq 4.5$ near $L \sim 5$ during disturbed periods (Agapitov et al., 2019; Mourenas et al., 2023; Mourenas, Zhang, et al., 2022).

To have sufficient statistics, we average ELFIN data over $\sim 20-30$ spacecraft spin periods (each spin period lasting 3 s) in the same L-shell domain, keeping all the available data (if J_{prec} is of the order of noise level, it is put to 0; see details in Angelopoulos et al., 2023). We focus on the $\sim 4-14$ MLT sector where chorus wave power is strong up to the middle latitudes where cyclotron resonance with 80–600 keV electrons near the loss cone occurs, leading to their precipitation into the atmosphere (Agapitov et al., 2018; Meredith et al., 2020). Moreover, we only use ELFIN data in a fixed, narrow range of MLT (and longitude) during each storm, because the trapped or quasitrapped electron flux measured there above the loss cone during periods of significant wave-driven pitch-angle diffusion varies in time smoothly and coherently with the trapped equatorial electron flux (Mourenas et al., 2021; Shane et al., 2023), in agreement with quasi-linear theory (Kennel & Petschek, 1966). Finally, electron fluxes measured at low altitude are averaged over $\Delta L \sim 1$, to take into account the typical equatorial size, $\Delta L \approx 0.5$, of an active region of chorus waves at $\sim 4-16$ MLT and $L \in [4.5, 6.5]$ (Agapitov et al., 2021) and the spreading of chorus rays along their propagation, by up to $\Delta L \approx 0.5$ at middle latitudes (Chen et al., 2013).

To estimate the effective precipitating flux $J_{prec}(t)$ due to chorus wave-driven pitch-angle diffusion, the electron flux $J_{back}(t)$ backscattered into the loss cone by the atmosphere in the conjugate region along the same field line has to be subtracted from the total measured precipitating flux $J_{prec, meas}(t)$. As in previous work (Mourenas et al., 2021), this is done using the backscattered flux $J_{up}(t)$ measured by ELFIN within the anti-loss-cone as an estimate of $J_{back}(t)$ in the conjugate region on the same field line (assuming symmetry over time scales much longer than an electron bounce period), giving $J_{prec}(t) = J_{prec, meas}(t) - J_{up}(t)$. Note that $J_{prec, meas}(t)$, $J_{up}(t)$, and $J_{prec}(t)$ are averaged over the loss cone and anti-loss-cone.

Two different versions of the time-averaged precipitating-to-trapped electron flux ratio J_{prec}/J_{trap} can be calculated, using the trapped or quasi-trapped electron flux J_{trap} measured by ELFIN CubeSats just above the loss cone:

$$\frac{J_{prec1}}{J_{trap}} = \frac{\langle J_{prec}^2 \rangle^{1/2}}{\langle J_{trap} \rangle}, \quad \frac{J_{prec2}}{J_{trap}} = \frac{\langle J_{prec} \rangle}{\langle J_{trap} \rangle}, \tag{1}$$

where each average is performed over roughly 30 ELFIN spins. In Equation 1, we build on the fact that J_{trap} is usually only moderately varying over such short averaging periods, whereas J_{prec} and $J_{prec}J_{trap}$ can strongly vary in the presence or absence of particularly intense chorus wave bursts (Mourenas et al., 2021; Mourenas, Zhang, et al., 2022). In addition, taking the time-averages of J_{prec} and J_{trap} prior to taking their ratio should result in robust estimates of that time-averaged ratio, mitigating potential time-aliasing effects on $J_{prec}J_{trap}$ due to the limited resolution in spacecraft spin-phase and the larger number of spin-phase sectors in the loss-cone than outside it (Angelopoulos et al., 2023). In Section 2.4, we will show that the chorus wave power gain G(t) can be inferred based on the measured time-averaged $J_{prec}J_{trap}$ given in Equation 1 and we will discuss the usefulness of the root-mean-squared and plain average versions of this flux ratio.

2.4. Using Quasi-Linear Theory to Infer Wave Power Gain

A basic result of quasi-linear diffusion theory is that the wave-driven electron pitch-angle diffusion rate near the loss cone, $D_{\alpha\alpha}$, is proportional to the magnetic wave power B_w^2 (Kennel & Petschek, 1966; Lyons et al., 1971).

MOURENAS ET AL. 4 of 21

This fundamental result of quasi-linear theory, based on the two assumptions of low wave amplitudes and incoherent waves, has been verified in test particle simulations for realistic, not too high wave amplitudes (Tao et al., 2012), and it remains approximately correct in an intermediate regime between quasi-linear and non-linear wave-particle interaction, corresponding to most of the short and intense chorus wave packets observed in the Earth's outer radiation belt (An et al., 2022; Artemyev, Mourenas, et al., 2022; Gan et al., 2022; Mourenas, Zhang, et al., 2022; Zhang, Agapitov, et al., 2020). Therefore, the increase of wave power gain G from time t_i to time t_{i+1} can be simply written as:

$$G(t_{i+1}) - G(t_i) = \ln\left(\frac{D_{aa}(t_{i+1})}{D_{aa}(t_i)}\right).$$
 (2)

Quasi-linear theory further indicates that J_{prec}/J_{trap} is approximately proportional to the square root of D_{aa} (Kennel & Petschek, 1966; Mourenas et al., 2021, 2023). Therefore, the quantity $(J_{prec1}/J_{trap})^2$ obtained from Equation 1 can theoretically provide a better estimate of wave power B_w^2 than $(J_{prec2}/J_{trap})^2$ when the time-averaging interval (or equivalently, the number of data points) is sufficiently large. But using both J_{prec1}/J_{trap} and J_{prec2}/J_{trap} can provide upper and lower bounds to the actual electron precipitation rate and wave power (see Section 2.5).

To estimate the wave power gain G(t) and its relationship to the equatorial trapped electron flux J_{trap} ($\alpha_0 = 90^\circ$) based on ELFIN CubeSat measurements, we need to calculate J_{prec1}/J_{trap} and J_{prec2}/J_{trap} at different successive times t_i during each storm. Assuming a quasi-equilibrium pitch-angle electron distribution at 0.08-0.6 MeV (as justified by previous works, see Mourenas et al., 2021; Shane et al., 2023), quasi-linear theory (Kennel & Petschek, 1966; W. Li et al., 2013) shows that the average precipitating to trapped flux ratio measured at ELFIN CubeSats can be approximately written as $J_{prec}/J_{trap} \simeq 1.3/(z_0 + z_0^2/200)$ (Mourenas et al., 2023), equivalent to:

$$z_0 \simeq \left(10^4 + 260 \frac{J_{trap}}{J_{prec}}\right)^{1/2} - 100,$$
 (3)

with <25% error when J_{prec}/J_{trap} < 0.8, where $z_0 = 2\alpha_{0,LC}/(D_{\alpha\alpha}\tau_B)^{1/2}$, $\tau_B(E,L)$ is the electron bounce period and the wave-driven pitch-angle diffusion rate $D_{\alpha\alpha}(E,t)$ is calculated at the loss-cone angle $\alpha_{0,LC}(L)$.

The relationship between the average quasi-equilibrium trapped electron flux at a given equatorial pitch-angle $\alpha_0 > \alpha_{0,LC}$ and its level at $\alpha_0 = 90^\circ$ is also given by quasi-linear theory (Kennel & Petschek, 1966; Mourenas et al., 2023):

$$\frac{J_{trap}(\alpha_0 = 90^\circ)}{J_{trap}(\alpha_0)} \approx \frac{1 + \langle z_0 \rangle \frac{I_1(\langle z_0 \rangle)}{I_0(\langle z_0 \rangle)} \ln\left(\frac{1}{\sin \alpha_{0,LC}}\right)}{1 + \langle z_0 \rangle \frac{I_1(\langle z_0 \rangle)}{I_0(\langle z_0 \rangle)} \ln\left(\frac{\sin \alpha_0}{\sin \alpha_{0,LC}}\right)}, \tag{4}$$

where $\langle z_0 \rangle$ (roughly proportional to the average J_{trap}/J_{prec} in the investigated domain $0.004 < J_{prec}/J_{trap} < 0.8$) is given by Equation 3 using $J_{prec} = J_{prec2}$ from Equation 1, and where I_x denotes the modified Bessel function of the first kind. Substituting J_{trap} ($\alpha_0 \simeq 1.05 \ \alpha_{0,LC}$) measured just above the loss-cone by ELFIN into Equation 4 gives the equatorial trapped flux J_{trap} ($\alpha_0 = 90^\circ$, E, t).

The electron flux pitch-angle anisotropy s for a distribution of the form J_{trap} (α_0) = $\sin^{2s}\alpha_0$ (Summers et al., 2009) for $\alpha_0 = 10^\circ - 90^\circ$ (i.e., for most of the electron population providing the free energy for chorus wave growth, see Omura et al., 2008; Tao et al., 2017; Mourenas, Zhang, et al., 2022) can be similarly estimated based on quasilinear theory (Mourenas et al., 2023), giving:

$$s \simeq \ln\left(\frac{J_{trap}(10^\circ)}{J_{trap}(90^\circ)}\right) \cdot \left(\frac{1}{2\ln(\sin(10^\circ))}\right),\tag{5}$$

with J_{trap} (10°) given by Equation 4 based on the previously obtained J_{trap} (90°).

MOURENAS ET AL. 5 of 21

Besides, the relativistic theoretical gain Gth has been calculated by Summers and Shi (2014). Fitting numerical results in their Figure 3 for $\Omega_{pe}/\Omega_{ce}\approx 4.5$ (a typical value at $L\approx 5$, see Agapitov et al., 2019), gives a Kennel-Petschek trapped flux limit $J_{KP}(90^\circ)\simeq\eta~G_0/(s^BL^4E)$ e/cm²/s/sr/MeV, with E in MeV, $G_0=3$ the expected gain at the Kennel-Petschek limit, $\eta\approx 2.6\times 10^8$ e/cm²/s/sr for linear wave growth over a distance $\Delta s=LR_E$, and the exponent B of anisotropy s in this formula of $J_{KP}(90^\circ)$ is given by $B=\max{((0.4/E~[MeV])^{0.4},1)}$ from 0.1 to 0.8 MeV for a typical pitch-angle anisotropy $s\simeq 0.25-0.5$ during strong injections of energetic electrons at $L\approx 5$ (Mauk & Fox, 2010; Olifer et al., 2022). The increase of exponent B as E decreases is due to an approach to the minimum energy for cyclotron resonance, which increases J_{KP} for smaller E and s (Summers & Shi, 2014). Accordingly, the theoretical relativistic linear convective wave power gain G_{th} is approximately proportional to $J_{trap}(90^\circ)s^BL^4E$ for a fixed ratio $\Omega_{pe}/\Omega_{ce}\approx 4.5$.

At this point in our derivation, it is worth noting that the gain increase from t_i to t_{i+1} , denoted $\Delta G = G(t_{i+1}) - G(t_i)$, depends only, through Equation 2, on the ratio of the two $J_{prec}J_{trap}$ values obtained from measurements at t_i and t_{i+1} . Since this ratio of two $J_{prec}J_{trap}$ values is independent of J_{trap} (it depends only on the ratio of resonant wave powers at these two times), ΔG is also independent of J_{trap} . Therefore, the Kennel-Petschek assumption of a wave power gain G increasing linearly with the theoretical linear wave power gain G_{th} , which is proportional to J_{trap} , can be tested by comparing at various times the inferred ΔG with ΔG_{th} . If ΔG increases roughly linearly with ΔG_{th} , it will mean that G increases roughly linearly with the theoretical gain G_{th} .

However, this does not yet provide us an estimate of the absolute value of G(t) at a given time. To derive such an estimate, it is reasonable to assume that the actual wave power gain G will be proportional to the theoretical linear convective wave power gain G_{th} , as in the derivation of the Kennel-Petschek flux limit (Kennel & Petschek, 1966; Shklyar & Matsumoto, 2009; Summers & Shi, 2014), giving $G(t_{i+1})/G(t_i) = G_{th}(t_{i+1})/G_{th}(t_i)$. This immediately yields $G(t_{i+1}) - G(t_i) = (G_{th}(t_{i+1})/G_{th}(t_i) - 1)G(t_i)$. Combining this relationship with the preceding equations, for a fixed E and a fixed E, the wave power gain G at each time E is given by:

$$G(t_{i}) = \ln \left[\left(\frac{z_{0}(t_{i})}{z_{0}(t_{i+1})} \right)^{2} \right] \cdot \left(\frac{J_{trap}(90^{\circ}, t_{i+1}) s(t_{i+1})^{B}}{J_{trap}(90^{\circ}, t_{i}) s(t_{i})^{B}} - 1 \right)^{-1},$$

$$G(t_{i+1}) = G(t_{i}) + \ln \left[\left(\frac{z_{0}(t_{i})}{z_{0}(t_{i+1})} \right)^{2} \right],$$

$$(6)$$

where values of z_0 , J_{trap} , s, and B at fixed E and L are used. In Equation 6, z_0 is given by Equation 3 using either $J_{prec} = J_{prec2}$, whereas J_{trap} (90°) and s are given by Equations 4 and 5 using always $J_{prec} = J_{prec2}$. To calculate G(t) at fixed L and E, we only keep times t_i and t_{i+1} such that the following inequalities are satisfied: $G(t_{i+1}) > G(t_i)$, J_{trap} (90°, t_{i+1}) $> J_{trap}$ (90°, t_i), and J_{trap} (90°, t_{i+1}) $s(t_{i+1})^B > J_{trap}$ (90°, t_i) $s(t_i)^B$. We calculate $G(t_i)$ from $E \ge 0.1$ MeV up to some energy $E \le 0.6$ MeV, and only when $J_{prec}(t_i) > 100$ e/cm²/s/sr/MeV, $J_{trap}(90^\circ, t_{i+1}) > 1.5$ $J_{trap}(90^\circ, t_i)$, and $J_{trap}(t_i) > 1.2$, to ensure a good accuracy.

Let us emphasize that wave power gains are inferred only by pairs $(G(t_i), G(t_{i+1}))$. For example, we can infer a first pair P_1 of gains $G(t_1, P_1)$ and $G(t_2, P_1)$ from measurements at t_1 and t_2 and, separately, another pair P_2 of gains $G(t_2, P_2)$ and $G(t_3, P_2)$ from measurements at t_2 and t_3 . These two pairs of gains are partly independent of each other, because measurements at t_1 and t_3 are independent of each other. Based on the assumption, used to derive Equation 6, that G is proportional to G_{th} and $J_{trap}(90^{\circ})$, we will necessarily get a linear increase of G(t) with G_{th} and $J_{trap}(t)$ for each pair of gains. However, Equation 2 indicates that $\Delta G(P_1) = G(t_2) - G(t_1)$ only depends on the variation of J_{pred}/J_{trap} and, consequently, is independent of $\Delta G(P_2)$ and of the absolute levels of J_{trap} (90°, t) and $G_{th}(t)$. Therefore, when examining the above-discussed two successive pairs P_1 and P_2 of inferred gains, the variation of G(t) from t_1 to t_3 as I_{trap} and G_{th} increase, given by Equation 6, may not be a monotonous increase, and the final gain $G(t_3) = \Delta G(P_2) + \Delta G(P_2)/(G_{th}(t_3)/G_{th}(t_2) - 1)$ can even become smaller than the initial gain $G(t_1) = \Delta G(P_1)/(G_{th}(t_2)/G_{th}(t_1) - 1)$ for a sufficiently small $\Delta G(P_2)$, corresponding to a sufficiently weak increase of I_{pre}/J_{trap} from t_2 to t_3 compared with its increase from t_1 to t_2 . This means that plotting the variation of G as a function of G_{th} for three or more independent pairs $(G(t_i), G(t_{i+1}))$ obtained at different times (or at different energies E or L-ranges) should indicate the actual dependence of the measured gain G on the theoretical gain G_{th} and J_{trap} . It can also help to verify the Kennel-Petschek assumption of a maximum gain $G_0 \approx 3$ at the flux limit J_{KP} .

MOURENAS ET AL. 6 of 21

The chorus wave power gain G(t) near the magnetic equator can be estimated using Equations 1–6 based only on low altitude ELFIN CubeSat measurements of precipitating, backscattered, and trapped electron flux, without any wave measurement. It is worth noting that, in deriving Equation 6, we made use of normalized z_0 (t_i) and flux values. An advantage of this method, previously used for electromagnetic ion cyclotron (EMIC) waves (Angelopoulos et al., 2023), is that such a normalization leads to a cancellation of all parameters in z_0 that remain approximately constant during the examined time interval, such as the plasma frequency to gyrofrequency ratio or the wave frequency to gyrofrequency ratio (Mourenas et al., 2023). As a result, the wave power gain near the magnetic equator can be inferred from low-altitude measurements alone, without additional plasma or wave measurements in the equatorial and mid-latitude regions where wave generation and electron precipitation take place.

2.5. Main Assumptions and Quantification of Uncertainties

The present method, like the Kennel-Petschek model (Kennel & Petschek, 1966; Summers et al., 2009), assumes that electrons in a given energy range $\approx E \pm \Delta E/2$, with $\Delta E/E \approx 40\%$ the full width of ELFIN energy channels (Angelopoulos et al., 2020) and $E \in [80, 600]$ keV, are providing (via their high $\alpha_0 > 60^\circ$ part) the free energy for chorus wave growth near the magnetic equator and are subsequently progressively precipitated into the atmosphere (at low α_0) mainly through cyclotron resonance at middle latitudes with the same waves (of similar frequencies ω). Averaging over the finite width ΔE of energy channels should make this approximation even more reasonable.

Based on known dependencies of z_0 and $D_{\alpha\alpha}$ on wave and plasma parameters (Mourenas et al., 2014), we need to assume that the equatorial plasma frequency to gyrofrequency ratio, $\Omega_{pe0}/\Omega_{ce0}\approx 4-5$ at $L\sim 5$, remains roughly constant over the investigated time interval, in agreement with statistical observations at 4–14 MLT during events with $AE \in [100, 1,000]$ nT (Agapitov et al., 2019; Sheeley et al., 2001), and that the wave power distribution as a function of normalized frequency ω/Ω_{ce0} remains approximately constant during the same time interval.

In addition, we must assume that the wave power ratio $B_w^2(t_{i+1})/B_w^2(t_i)$ at latitudes $\lambda \sim 10^\circ - 30^\circ$ of cyclotron-resonant electron precipitation is approximately the same as at $\lambda < 10^\circ$ where chorus wave growth takes place. This reasonable requirement is equivalent to assuming a similar Landau damping of the waves at t_i and t_{i+1} along their propagation to middle latitudes, consistent with statistical observations at L = 4 - 6 and 4 - 14 MLT showing a similar latitudinal distribution of chorus wave power from Kp = 3 to Kp = 6 (Agapitov et al., 2018).

Finally, we wish to eliminate any bias related to random temporal fluctuations of J_{trap} and J_{prec}/J_{trap} , produced by sub-second chorus wave bursts, and to smooth out flux variations due to the spacecraft's relatively low sampling rate compared with physical phenomena (Zhang et al., 2022). Therefore, we need to average the measured electron fluxes over as much data as possible.

Nevertheless, a finite level of natural fluctuations of all physical quantities is unavoidable and we need to estimate the corresponding uncertainties on the inferred G. Based on the uncertainties ΔJ_{trap} and ΔJ_{prec} on the measured average fluxes, the uncertainty ΔG on the gain given in Equation 6 is:

$$\frac{\Delta G}{G} \approx \frac{2}{(G(t_{i+1}) - G(t_i))} \left(\frac{\Delta J_{prec}}{J_{prec}} + \frac{\Delta J_{trap}}{J_{trap}} \right) + \frac{\Delta J_{trap}(t_{i+1})}{J_{trap}(t_{i+1}) - \frac{s(t_i)^B}{s(t_i, \cdot)^B} J_{trap}(t_i)}.$$
 (7)

The relative variations of the trapped electron flux measured by ELFIN CubeSats are much less important than the relative variations of the much weaker precipitating electron flux (Mourenas et al., 2021; Mourenas, Zhang, et al., 2022). Since we usually have $(J_{trap}(t_{i+1}) - (s(t_i)/s(t_{i+1}))^B J_{trap}(t_i)) > J_{trap}(t_{i+1}) (G(t_{i+1}) - G(t_i))/20$, this gives $\Delta G/G \approx 2$ ($\Delta J_{prec}/J_{prec}/J(G(t_{i+1}) - G(t_i))$) to first order. Accordingly, a reasonable estimate of the uncertainty ΔG is given by the difference between the two values of G obtained by using the two different versions, J_{prec}/J_{trap} and J_{prec}/J_{trap} , of the average precipitating to trapped flux ratio given in Equation 1, corresponding to two different averages of J_{prec} .

Based on Equation 3, $D_{\alpha\alpha}(\alpha_{0,LC})$ is roughly proportional to J_{prec}^2 within the investigated domain $0.004 < J_{prec}/J_{prec}/J_{prec} < 0.8$. Consequently, for a sufficiently large and representative time-averaging interval, $J_{prec}^2 = \langle J_{prec}^2 \rangle$ should theoretically provide a more accurate estimate of the time-averaged $D_{\alpha\alpha}(\alpha_{0,LC})$ and G(t) than

MOURENAS ET AL. 7 of 21

 $J_{prec2}^2 = \langle J_{prec} \rangle^2$. Using J_{prec2}^2 should generally provide somewhat underestimated values of the time-averaged $D_{\alpha\alpha}(\alpha_{0,LC})$, but also of G(t), because the ratio $D_{\alpha\alpha}(t_{i+1})/D_{\alpha\alpha}(t_i)$ is prone to a stronger increase based on $\langle B_w^2 \rangle$ (each B_w^2 value corresponding to a ~ 3 s spin of ELFIN) than based on $\langle B_w \rangle^2$ when the high-intensity tail of chorus wave bursts increases (Zhang et al., 2019). On the other hand, for a realistic, limited time-averaging interval of $\sim 20-30$ ELFIN spins, J_{prec1}^2 can be more affected than J_{prec2}^2 by the presence of an outlier in the data, corresponding to an exceptionally intense wave burst (see examples of such ELFIN spectra in Tsai et al., 2023; Zhang et al., 2022). Sometimes, this can make J_{prec1}^2 less representative of the actual wave power distribution than J_{prec2}^2 , leading to temporal fluctuations of the inferred G(t) and giving less reliable estimates than J_{prec2}^2 . In Section 3, the two estimates of G(t) obtained from J_{prec1}^2 and J_{prec2}^2 will be plotted, to provide the uncertainty range of the inferred G(t).

2.6. Usefulness

This method allows to infer both the equatorial trapped electron flux J_{trap} (90°) and the equatorial wave power gain G from low-altitude electron flux data, based on quasi-linear theory. It provides the means for checking two key assumptions of the Kennel-Petschek model (Kennel & Petschek, 1966; Summers et al., 2009): (a) the exponential increase of the chorus wave power B_w^2 with J_{trap} (90°) at a given latitude of cyclotron resonance with electrons of energy E near the loss cone, equivalent to a linear increase of the wave power gain G with J_{trap} (90°), and (b) the existence of a fixed maximum gain, $G_0 \approx 3$, reached when J_{trap} (90°) attains its maximum level during a geomagnetic storm.

This method only requires low-altitude energy and pitch-angle resolved measurements of electron fluxes. But it can be supplemented by conjugate measurements near the magnetic equator or at middle latitudes on the same magnetic field line. For instance, chorus wave power gains G(t) and diffusion rates $D_{\alpha\alpha}(\alpha_{0,LC})$ inferred from ELFIN's measurements can be compared with other spacecraft measurements of chorus wave power around the equator.

In addition, one can use the $\Omega_{peo}/\Omega_{ceo}$ ratio from an empirical plasma density model (Sheeley et al., 2001) at $L \sim 5$ during moderate geomagnetic storms, and ω/Ω_{ceo} as a function of latitude from another statistical model (Agapitov et al., 2018), to estimate from the variation of J_{prec}/J_{trap} as a function of E the wave power B_w^2 as a function of the latitude of resonance with electrons of different energies near the loss cone. This could give an indication of the strength of Landau damping (Bell et al., 2002; Bortnik et al., 2007), which may partly compensate in G(t) the convective wave growth produced by J_{trap} at low latitudes.

3. Applications to Moderate Geomagnetic Storms

First, we examine the moderate 16-18 April 2021 geomagnetic storm, with minima of Dst and Sym - H indices of -54 and -61 nT, respectively, at 05 UT on 17 April, and an average Kp of 4 from 18 UT on 16 April to 13 UT on 18 April (see Figure 1). Such conditions typically correspond to strong and prolonged injections of energetic $\sim 50-150$ keV electrons from the plasma sheet (Birn et al., 1998; Gabrielse et al., 2014; X. Li et al., 1998; Turner et al., 2015) and sustained chorus wave-driven electron energization and precipitation into the atmosphere at $L \sim 4.5-6.5$ (Agapitov et al., 2018), leading to a strong increase of $\sim 0.1-2$ MeV trapped electron flux up to some upper limit (Hua, Bortnik, Chu, et al., 2022; Hua, Bortnik, & Ma, 2022; Mourenas, Artemyev, et al., 2022; Mourenas et al., 2023; Olifer et al., 2022). Using the SuperMag SME index as a good proxy for AE (Gjerloev, 2012) in an empirical plasmapause model based on AE (O'Brien & Moldwin, 2003) indicates that the plasmasphere remained at L < 4 over 5-7 MLT during the whole period displayed in Figure 1.

Figure 1b shows a strong increase, from 16 April (18 UT) to 18 April (13 UT) 2021, of the trapped or quasi-trapped 240 keV (black) and 500 keV (blue) electron flux J_{trap} , measured at an altitude of ~450 km by ELFIN A and B (filled and empty circles, respectively) at $L \in [4.5, 5.5]$ near 6 MLT. The corresponding precipitating to trapped flux ratio $J_{prec}/J_{trap} = J_{prec2}/J_{trap}$, displayed in Figure 1c, can fluctuate much more than J_{trap} over short time scales (as near 17 UT on 17 April or near 20 UT on 16 April), due to the presence or absence of high intensity chorus wave bursts at middle latitudes and microbursts (Chen et al., 2022; Zhang et al., 2022), or due to occasional bursts of highly oblique chorus waves (Artemyev, Zhang, et al., 2022). In the following, we use ELFIN A data (filled circles) at 17:35 UT on 16 April, at 18:30 UT on 17 April, and at 13:10 UT on 18 April

MOURENAS ET AL. 8 of 21

- Los Ange, Wiley Online Library on [03/03/2024]. See the

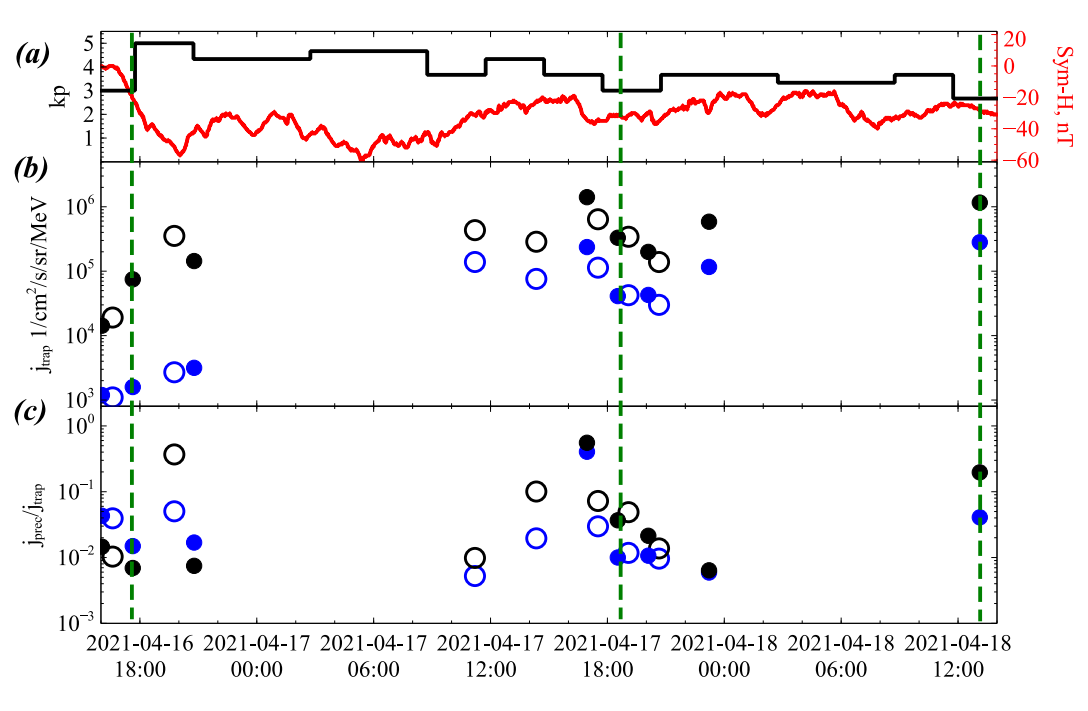


Figure 1. (a) Kp (black) and Sym - H (red) indices from 16 UT on 16 April to 14 UT on 18 April 2021. (b) Trapped (or quasitrapped) 240 keV (black) and 500 keV (blue) electron flux J_{trap} measured at low altitude by ELFIN A (filled circles) and ELFIN B (empty circles) at L = 4.5 - 5.5 and 5 - 7 MLT. (c) Precipitating-to-trapped 240 keV (black) and 500 keV (blue) electron flux ratio $J_{prec}/J_{trap} = J_{prec}/J_{trap}$ measured by ELFIN A (filled circles) and ELFIN B (empty circles) at L = 4.5 - 5.5 and 5 - 7 MLT. Vertical dashed green lines on 16, 17, and 18 April indicate the selected data used in the following figures.

(times indicated by vertical dashed green lines in Figure 1), which correspond to near-median trapped fluxes and precipitating-to-trapped flux ratios around those times, and exhibit increases in those quantities at 240 keV from 16 to 17 to 18 April.

Figures 2a, 2f, and 2k show the average precipitating to trapped electron flux ratio J_{prec1}/J_{trap} from Equation 1 at L=3.5-6.5 on 16, 17, and 18 April 2021, measured by ELFIN A near 6 MLT, as a function of electron energy. Figures 2b, 2g, 2l, and 2c, 2h, 2m show the chorus wave-driven electron quasi-linear pitch-angle diffusion rates $D_{\alpha\alpha}$ near the loss cone, inferred using Equation 3 from the measured J_{prec1}/J_{trap} and J_{prec2}/J_{trap} , respectively. Figures 2d, 2i, and 2n show the equatorial trapped electron fluxes J_{trap} ($\alpha_0 = 90^{\circ}$) inferred using Equation 4, and Figures 2e, 2j, and 20 show the pitch-angle anisotropy s estimated based on Equation 5.

Figure 2 shows that the precipitating to trapped flux ratio J_{prec1}/J_{trap} , the chorus wave-driven electron pitchangle diffusion rate $D_{\alpha\alpha}$ near the loss cone evaluated based on J_{prec1}/J_{trap} or J_{prec2}/J_{trap} , and the equatorial trapped flux J_{trap} (90°) progressively increased from 16 to 18 April, above 150 keV at L = 4.5 - 5.5 and at $\sim 80 - 300$ keV at L = 5.5 - 6.5. The observed increase of $D_{\alpha\alpha}$ indicates a strong increase of chorus wave power concomitant with the observed increase of trapped electron flux, in agreement with previous results that showed a statistical relationship between 80 keV electron flux and chorus wave power measured near the equator at $L \approx 5$ by the Van Allen Probes during geomagnetic storms (Chakraborty et al., 2022). The trapped flux J_{trap} (90°) increased much less between 17 and 18 April than between 16 and 17 April, indicating a probable approach to a flux limit. On 18 April, J_{trap} (90°) was indeed within a factor of ~2 of the upper flux limit observed during storms in 2013–2018 at \sim 100 – 600 keV and $L \sim 5.0 - 5.5$ (Hua, Bortnik, & Ma, 2022). A previous, more limited investigation of the 16–18 April 2021 storm at $L \sim 5$ has shown that the trapped flux J_{trap} (90°, E) reached on 18 April an energy spectrum shape at ~100 - 600 keV very similar to an upper flux limit $I_{UL}(E)$ corresponding to a dynamical equilibrium with steady-state attractor in the presence of sustained injections and both pitch-angle and energy diffusion by chorus waves (Mourenas et al., 2023). This upper flux limit $J_{II}(E)$ corresponds to a balance between the total number of injected and precipitated electrons per second; its functional shape versus energy is often close to the shape of the Kennel-Petschek flux limit $J_{KP}(E)$ at 100 - 500 keV (Mourenas et al., 2023).

MOURENAS ET AL. 9 of 21

from https://agupubs.onlinelibrary.wiley.com/doi/10.1029/2023JA032193 by University of California

Los Ange, Wiley Online Library on [03/03/2024]. See the Terms

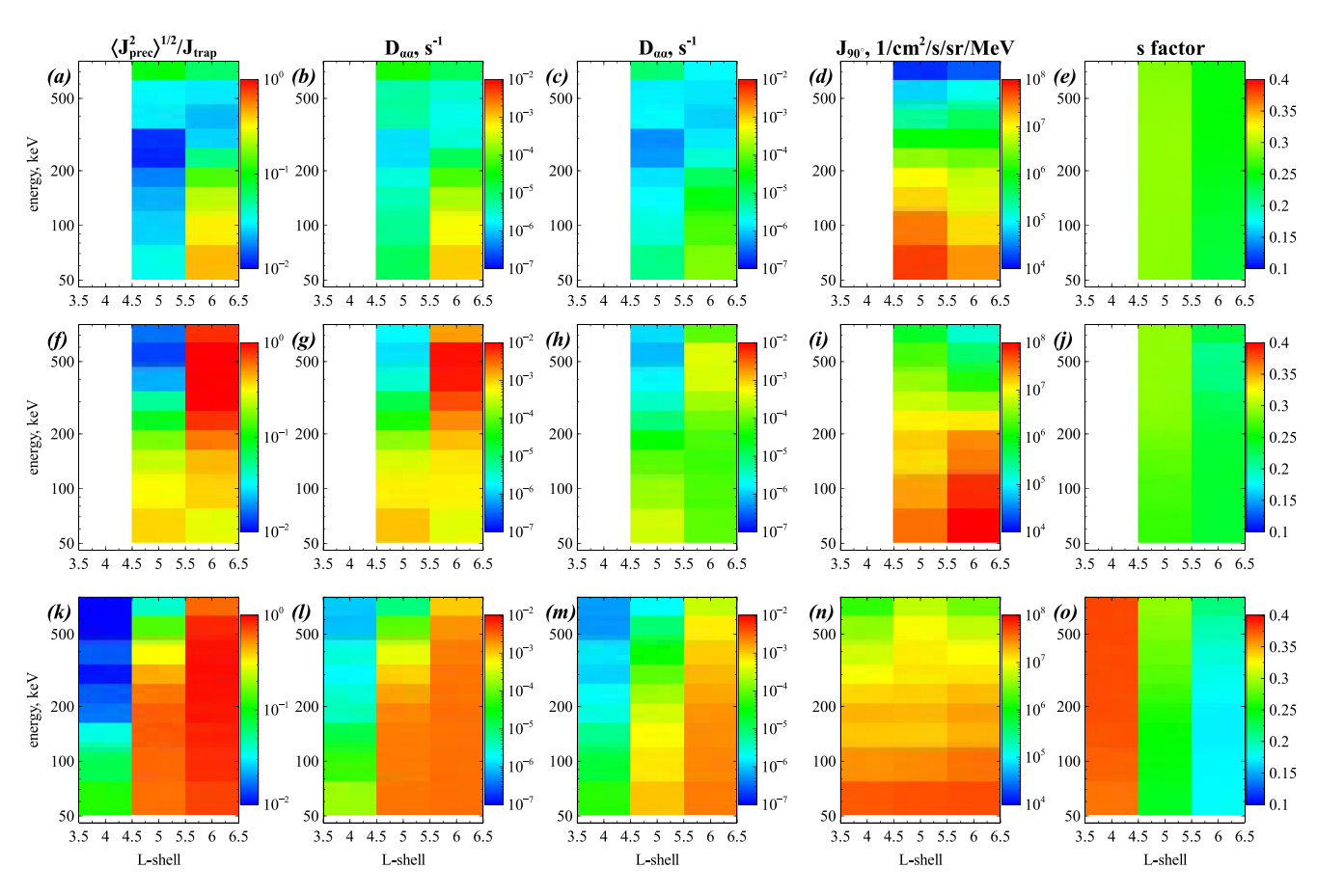


Figure 2. (a) Average precipitating to trapped electron flux ratio J_{prec1}/J_{trap} from Equation 1 at L=3.5-6.5 on 16 April 2021 (near 18 UT), based on ELFIN CubeSat low-altitude electron flux measurements near 6 MLT, as a function of electron energy. (b) Chorus wave-driven electron pitch-angle diffusion rate $D_{\alpha\alpha}$ near the loss cone inferred using Equation 3 and J_{prec1}/J_{trap} . (c) Same as (b) using J_{prec2}/J_{trap} from Equation 1. (d) Equatorial trapped electron flux estimated based on Equation 4. (e) Pitch-angle anisotropy s inferred using Equation 5 during the same period as in (a,b,c,d) (f)–(j) and (k–o) Same as (a)–(e) based on ELFIN measurements on 17 April (near 18 UT) and on 18 April 2021 (near 13 UT), respectively.

Figures 2e, 2j, and 2o further show that the pitch-angle anisotropy s decreased from ~ 0.3 to $\sim 0.2-0.25$ from 16 to 18 April, as expected in the presence of stronger pitch-angle diffusion (Kennel & Petschek, 1966; Olifer et al., 2022). Pitch-angle diffusion is found to be stronger at higher L-shells, consistent with statistical chorus wave models (e.g., see Agapitov et al., 2018). The relatively low pitch-angle anisotropy $s \sim 0.25$ on 18 April is close to the level $s \sim 0.3$ usually recorded when the trapped flux has increased up to the Kennel-Petschek limit J_{KP} (Mauk & Fox, 2010; Olifer et al., 2022). This confirms that J_{trap} (90°) was probably close to J_{KP} at $\sim 100-300$ keV at the end of this event, as during various similar events in 2016–2017 (Olifer et al., 2022).

Next, we focus in Figure 3 on the 180-300 keV energy range where the three inequalities J_{trap} (90°, t_{i+1}) $\gtrsim 1.5$ J_{trap} (90°, t_i), $J_{prec} > 100$ e/cm²/s/sr/MeV, and z_0 (t_i)/ z_0 (t_{i+1}) > 1.2 are usually satisfied, which should correspond to more reliable estimates of the chorus wave power gain G(t) than at other energies (see Section 2). Figure 3 shows the temporal variation of G(t) during this storm at 180 keV, 240 keV, and 300 keV, within two L-shell ranges (4.5 – 5.5 and 5.5 – 6.5), inferred from ELFIN measurements using either J_{prec1}/J_{trap} (circles linked by solid lines) or J_{prec2}/J_{trap} (triangles linked by dashed lines). Such G(t) values are calculated using Equation 6 over the periods 16-17 April (red), 17-18 April (blue), and 16-18 April (black), giving different estimates on each day. Note that G(t) values are calculated and plotted only when the above-listed three inequalities are satisfied, to remove unreliable estimates.

For 90% of the G(t) values in Figure 3, the two different estimates of G, $G_1 = G(J_{prec1})$ and $G_2 = G(J_{prec2})$, are both simultaneously available and correspond to an uncertainty $\Delta G/G \approx |G_1 - G_2|/(|G_1 + G_2|/2)$ smaller than

MOURENAS ET AL. 10 of 21

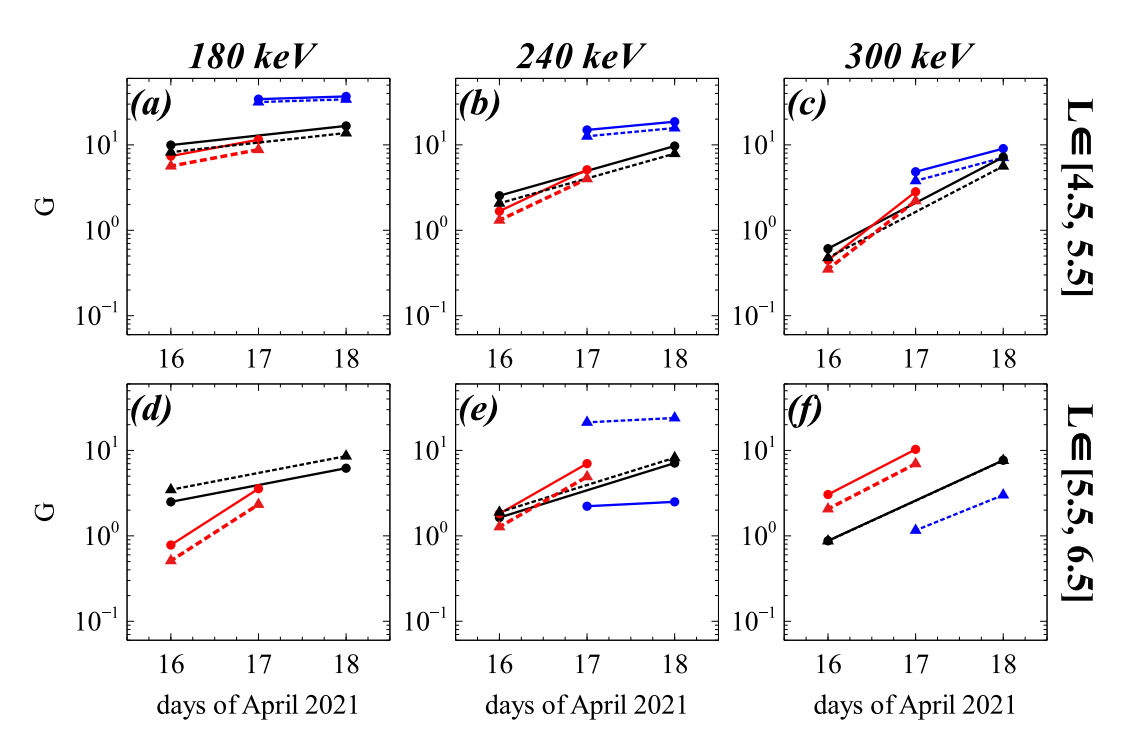


Figure 3. (a) Chorus wave power gain G(t) at L = 4.5 - 5.5 on 16–18 April 2021, inferred from ELFIN low-altitude electron flux measurements at 180 keV near 6 MLT. The different G(t) values obtained using J_{prec1} and J_{prec2} are shown by circles (linked by solid lines) and triangles (linked by dashed lines), respectively. The periods 16–17 April (red), 17–18 April (blue), 16–18 April (black) are examined separately, providing different G(t) estimates at each time. (b),(c) Same as (a) for 240 and 300 keV, respectively. (d,e,f) Same as (a,b,c) at L = 5.5 - 6.5.

40%, lending credence to these estimates. In addition, the different G estimates obtained at a given time, energy, and L, by analyzing different periods (16–17, 17–18, or 16–18 April) of the same event, usually differ by a factor ≈ 2 or less. This suggests that wave and plasma parameters other than wave power probably varied weakly during this event (see Section 2.5).

Figure 3 directly shows that G(E, t) steadily increased over the course of this storm at all energies $E \in [180, 300]$ keV and $L \sim 4.5 - 6.5$, although the stronger increase of G(t) on 16–17 April (red lines) than on 17–18 April (blue lines) in Figures 3a–3c indicates a saturation of G on 17–18 April. These results therefore confirm the presence of a steep increase of chorus wave power as the trapped electron flux increased during the storm, in agreement with the assumption made in the Kennel-Petschek model.

Regrouping all G(t) values from Figure 3 on each day further shows that the median and mean values of G(t) increased from ~ 1.7 and ~ 2.5 on 16 April, to ~ 5 and ~ 7 on 17 April, up to ~ 8 and ~ 13 on 18 April, respectively. This corresponds to a steep, exponential increase of the average chorus wave power $B_w^2(t) \approx \exp[G(t)]$. However, it is worth emphasizing that at the start of this event, on 16 April, the median and mean inferred $G \sim 1.7 - 2.5$ were already close to the maximum gain $G_0 = 3$ assumed at the Kennel-Petschek flux limit (Kennel & Petschek, 1966; Summers et al., 2009; Summers & Shi, 2014). The median and mean inferred G strongly increased during the storm, reaching $G \sim (1.7-2.3) \times 3$ on 17 April and $\sim (2.7-4.3) \times 3$ on 18 April. These results suggest that the actual chorus wave power gain G significantly exceeded the maximum gain $G_0 = 3$ usually assumed at the Kennel-Petschek flux limit $J_{trap} \sim J_{KP}$ (Kennel & Petschek, 1966; Summers et al., 2009) during roughly one day, from 17 to 18 April 2021. Accordingly, the actual Kennel-Petschek flux limit J_{KP} , which is proportional to G (Kennel & Petschek, 1966; Summers et al., 2009; Summers & Shi, 2014), could have been ~ 3 times higher during this storm than usual estimates relying on a maximum level max(G) = $G_0 = 3$.

By construction, Equation 6 assumes a linear variation of the inferred G with the theoretical linear convective chorus wave power gain $G_{th} \approx J_{trap} (90^\circ) s^B L^4 E/\eta$ (Summers & Shi, 2014), with η a constant, between two times t_i

MOURENAS ET AL. 11 of 21

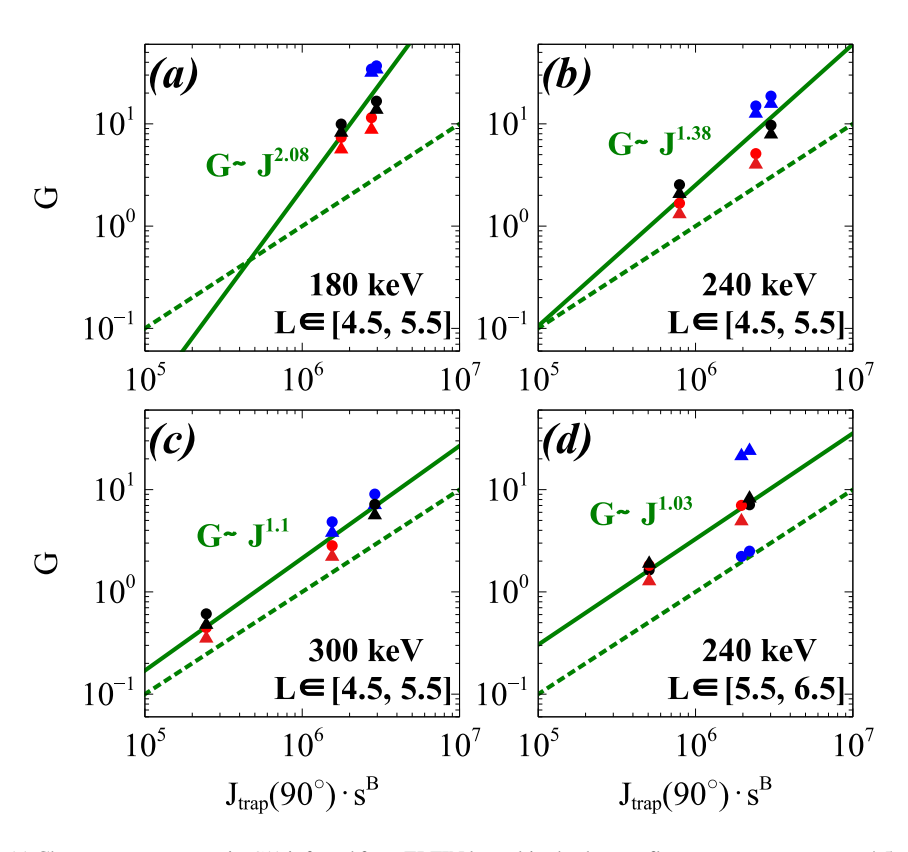


Figure 4. (a) Chorus wave power gain G(t) inferred from ELFIN low-altitude electron flux measurements at L=4.5-5.5 and 180 keV, as a function of J_{trap} (90°, t)s^B at fixed E and L on 16–17–18 April 2021 (with J_{trap} in e/cm²/s/sr/MeV). G(t) is obtained using J_{prec1} (circles) and J_{prec2} (triangles), over periods 16–17 April (red), 17–18 April (blue), and 16–18 April (black). A dotted green line shows the theoretical trend corresponding to a constant ratio $G(t)/(J_{trap}(90^{\circ}, t)s^{B})$, and a solid green line shows a least squares power-law fit. (b),(c) Same as (a) for 240 and 300 keV, respectively. (d) Same as (a) for 240 keV at L=5.5-6.5.

and t_{i+1} corresponding to two same symbols of same color in a same panel of Figure 3. However, both $G(t_{i+1}) - G(t_i)$ and the inferred $G(t_i)$ can freely vary from one time interval (t_i, t_{i+1}) to another, corresponding to different colors in each panel of Figure 3, or from one energy E to another or from one L-range to another, corresponding to different panels in Figure 3. Plotting a best least squares fit to 3 or more of such independent groups of data points can therefore reveal the actual dependence of G on $J_{trap}(90^\circ)s^BL^4E$.

Since G_{th} is proportional to J_{trap} $(90^\circ)s^B$ for fixed E and L, we first show in Figure 4 the inferred gain G as a function of J_{trap} $(90^\circ)s^B$ for separate (L, E) pairs, each of which corresponds to 12 available estimates of G representing 3 independent quadruplets of points. The results in Figure 4 are roughly consistent with a linear increase of the inferred gain G with the theoretical gain G_{th} , which varies like J_{trap} $(90^\circ)s^B$ at fixed E and E0, with best least squares fits (solid green lines) $G = \beta \cdot \left[J_{trap}(90^\circ)s^B\right]^\alpha$ with β a constant and $\alpha \simeq 1.03$, 1.38, 1.1 for 240 keV at E1 = 5.5 - 6.5 and 240 and 300 keV at E3 = 4.5 - 5.5, respectively, and E3 for 180 keV at E3 = 4.5 - 5.5.

Next, all the data in Figure 3 (except for two points in Figure 3f of unknown uncertainty without estimates based on J_{prec1}), corresponding to 16 independent quadruplets of points, are used together in Figures 5a and 5b. First, Figure 5a shows G as a function of J_{trap} (90°) s^BL^4E (with J_{trap} in e/cm²/s/sr/MeV and E in MeV). It demonstrates that the inferred gain G increases approximately linearly with the theoretical gain, with a best least squares fit $G = \beta \cdot \left[J_{trap}(90^\circ)s^BL^4E/10^8\right]^\alpha$ with $\beta = 1.7$, $\alpha = 0.97$, and 68% confidence intervals 0.83 < α < 1.11 and 1.1 < β < 2.3. Although the Pearson correlation coefficient is weak, R = 0.23, this linear correlation is statistically significant at a 93% confidence level (Press et al., 2007). The Spearman rank-order correlation coefficient, $R_s = 0.56$, confirms the presence of a statistically significant monotonic relationship between inferred and theoretical gains at a 93% confidence level.

MOURENAS ET AL. 12 of 21

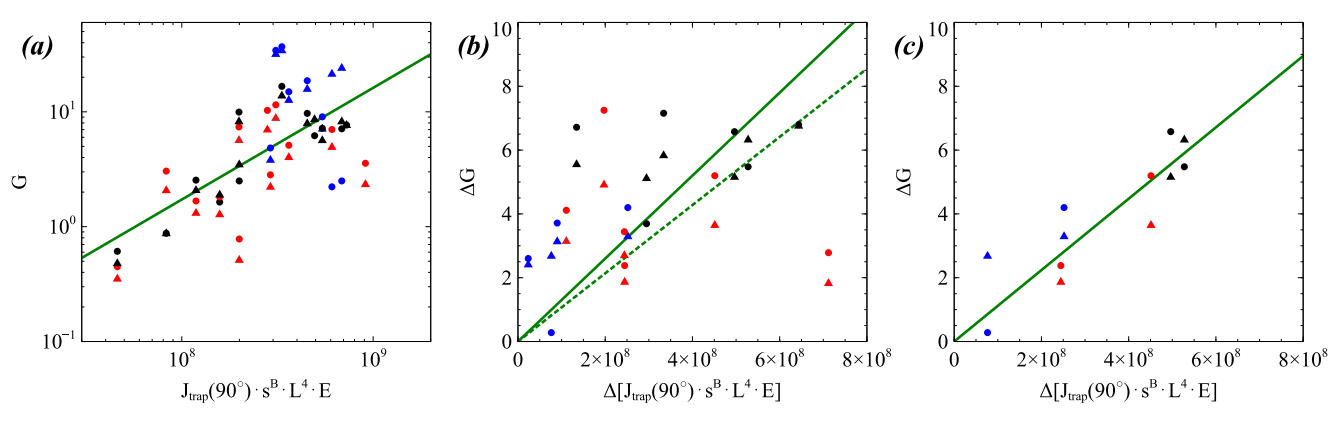


Figure 5. (a) Chorus wave power gain G as a function of $J_{trap}(90^\circ)s^BL^4E$ (with J_{trap} in e/cm²/s/sr/MeV and E in MeV) on 16–18 April 2021 inferred from ELFIN lowaltitude electron flux measurements at 180 – 300 keV and $L \sim 4.5$ – 6.5. G is obtained using J_{prec1} (circles) and J_{prec2} (triangles), over 16-17 April (red), 17-18 April (blue), and 16-18 April (black). The solid green curve shows the best least squares power-law fit, $G = 1.7 \cdot \left(J_{trap}(90^\circ)s^BL^4E/10^8\right)^{0.97}$. (b) ΔG as a function of $\Delta(J_{trap}(90^\circ)s^BL^4E)$ on 16–18 April, with the best least squares linear fit $\Delta G = 1.07 \cdot \Delta(J_{trap}(90^\circ)s^BL^4E/10^8)$ with R = 0.337 (dashed green line). After excluding two outliers in the lower right corner, the best fit becomes $\Delta G = 1.3 \cdot \Delta(J_{trap}(90^\circ)s^BL^4E/10^8)$ with R = 0.6 (solid green line). (c) Same as (b) but keeping only (E, L) pairs in Figure 3 with G values most consistent with each other, at 300 keV and $L \sim 5$ and 240 keV and $L \sim 6$. The best least squares linear fit is $\Delta G = 1.12 \cdot \Delta(J_{trap}(90^\circ)s^BL^4E/10^8)$ with R = 0.87 (solid green line).

A second estimate of the relationship between G and J_{trap} (90°) s^BL^4E during this storm is obtained in Figure 5b, which shows the variation ΔG of G between t_i and t_{i+1} as a function of the variation $\Delta (J_{trap} (90^\circ) s^BL^4E)$ of the theoretical linear gain. All 32 values displayed in Figure 5b are directly inferred from ELFIN measurements using only Equations 2–5, without any assumption on the variation of G(t) with trapped flux between t_i and t_{i+1} . The best least squares linear fit (dashed green line) is equivalent to a scaling $G = 1.07 \cdot (J_{trap} (90^\circ) s^BL^4E/10^8)$ similar to the scaling in Figure 5a, with a correlation coefficient R = 0.337. The Student t-test value for this correlation, $t = (n-2)^{1/2}R/(1-R^2)^{1/2} = 1.96$ for n = 32 points, implies that there is a significant linear relationship between G and $J_{trap} (90^\circ) s^BL^4E$ at a confidence level of 94% (Press et al., 2007). Moreover, 2 points in the lower right corner of Figure 5b, which are located far away from all the other points, are identified as outliers at a ~75% confidence level using the one-tail generalized Extreme Studentized Deviate test (Rosner, 1983) on the right-hand-side of the best fit. After excluding these 2 probable outliers, we get a best least squares linear fit $G = 1.3 \cdot (J_{trap} (90^\circ) s^BL^4E/10^8)$ (solid green line), with a significant correlation coefficient R = 0.6. This best fit is very close to the best fit in Figure 5a.

As in the case of the two outliers in Figure 5b, shown by red symbols in Figure 3d, there are sometimes significant discrepancies between inferred G(t) values for a given (E, L) pair in Figure 3. Consequently, we plot again ΔG as a function of $\Delta(J_{trap}(90^\circ)s^BL^4E)$ in Figure 5c, but here we keep only the (E, L) pairs from Figure 3 with inferred G values most consistent with each other (based on their respective uncertainties given by the difference between G values inferred using J_{prec1}/J_{trap} and J_{prec2}/J_{trap}), at 300 keV and $L \sim 5$ and at 240 keV and $L \sim 6$. Such inferred G values are expected to be the most reliable, since each of them has been obtained in two different ways, using two different pairs of electron flux measurements. This yields a best least squares linear fit $G = 1.12 \cdot \Delta(J_{trap}(90^\circ)s^BL^4E/10^8)$ with a high correlation coefficient R = 0.87 (solid green line), close to the best fits in Figures 5a and 5b. Therefore, the results in Figure 5 are consistent with the Kennel-Petschek assumption (Kennel & Petschek, 1966; Summers & Shi, 2014) of a wave power gain G proportional to the theoretical linear convective gain G_{th} up to the upper flux limit when $J_{trap}(90^\circ)s^BL^4E \lesssim 7.5 \times 10^8$ and $J_{trap}(90^\circ) \lesssim 2.5 \times 10^7$ e/cm²/s/sr/MeV at 180-300 keV and L = 4.5 - 6.5.

However, one cannot exclude a saturation of G at higher J_{trap} (90°) values. A trapped flux J_{trap} (90°) $\simeq 5 \times 10^7$ e/cm²/s/sr/MeV, higher than on 18 April 2021, has been measured at 180 keV and $L \approx 5$ by the Van Allen Probes at the end of two similar events, on 29 September and 27 October 2016 (Hua, Bortnik, & Ma, 2022; Mourenas et al., 2023). A sufficiently high trapped flux J_{trap} (90°) may allow a simultaneous growth of chorus waves at various distant frequencies (Katoh & Omura, 2016; Kuzichev et al., 2019; Tao et al., 2020; Zhang et al., 2021), leading to wave resonance overlap and the formation of mainly short wave packets with saturated peak amplitudes $B_{w,peak} < 0.2$ nT (Mourenas, Zhang, et al., 2022), as for the majority of chorus wave packets in the inner

MOURENAS ET AL. 13 of 21

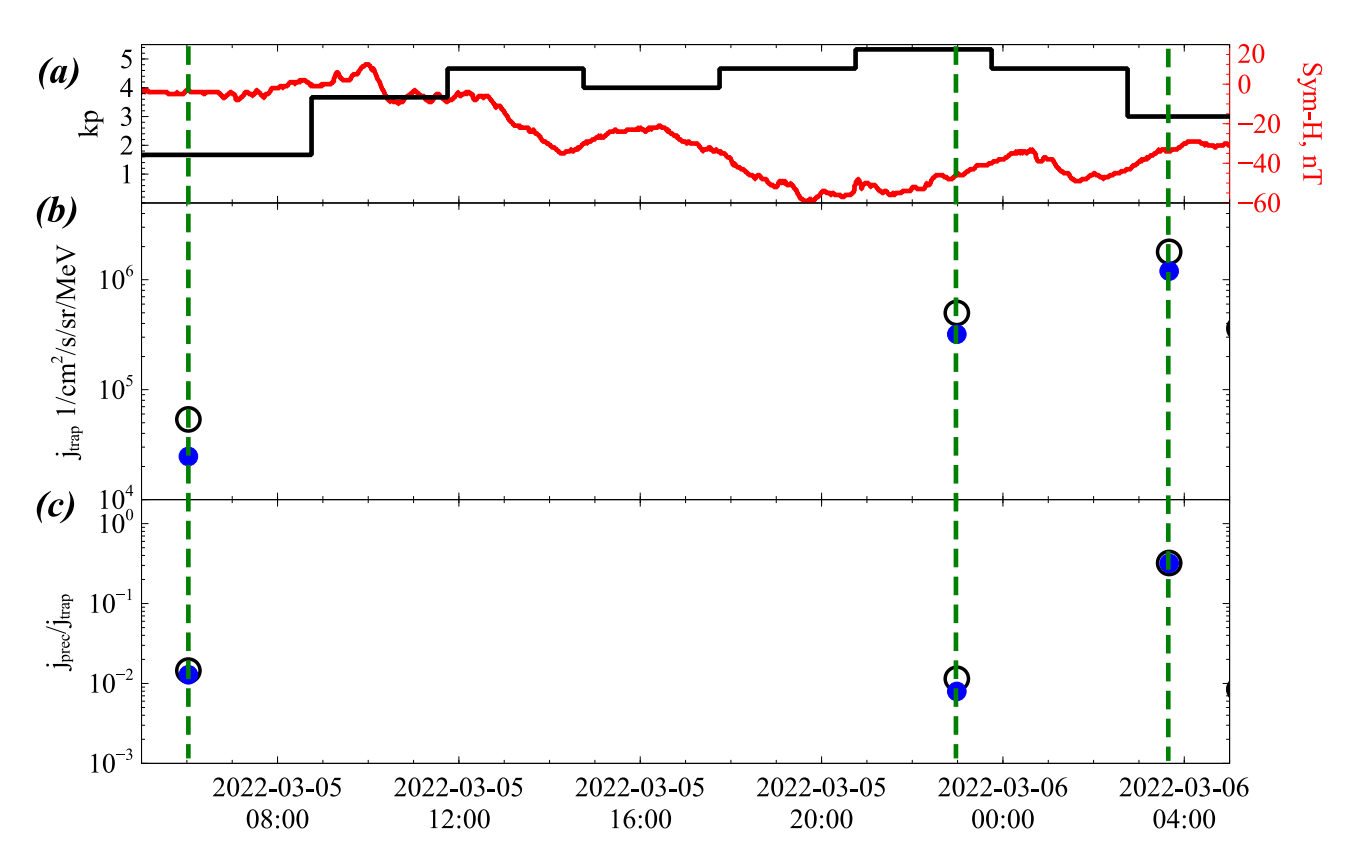


Figure 6. (a) Kp (black) and Sym - H (red) indices from 5 UT on 5 March to 5 UT on 6 March 2022. (b) Trapped (or quasi-trapped) 180 keV (black circles) and 240 keV (blue circles) electron flux J_{trap} measured at low altitude by ELFIN B at L = 4.5 - 5.5 and 14–16 MLT. (c) Precipitating-to-trapped 180 keV (black circles) and 240 keV (blue circles) electron flux ratio $J_{prec}/J_{trap} = J_{prec}/J_{trap}$ measured by ELFIN B at L = 4.5 - 5.5 and 14–16 MLT. Vertical dashed green lines indicate the data used in the following figure.

magnetosphere (Zhang et al., 2019; Zhang, Mourenas, et al., 2020). This effect, or a sufficiently strong reduction of anisotropy s as J_{trap} (90°) increases, might result in a saturation of G at very high trapped fluxes.

Next, we investigate a second, shorter event, the moderate 5–6 March 2022 geomagnetic storm, with a minimum Dst of -56 nT and a minimum Sym - H of -60 nT at 21 UT on 5 March, and an average Kp of \sim 4.3 from 9 UT on 5 March to 5 UT on 6 March (see Figure 6). Using the SME index as a proxy for AE in an empirical plasmapause model based on AE (O'Brien & Moldwin, 2003) shows that the plasmasphere remained at L < 4 over 14–16 MLT during the period displayed in Figure 6. At the three selected times (denoted by vertical green dashed lines) in Figure 6, there was no peak of the precipitating-to-trapped flux ratio $J_{prec}/J_{trap} > 0.5$ above 1 MeV in ELFIN B data at L = 4.5 - 5.5 and 14–16 MLT. This indicates that EMIC waves, which can sometimes be present in a high-density plume, were absent in the 14–16 MLT sector at these times (Angelopoulos et al., 2023). Figure 6 shows that the trapped 180–240 keV electron flux J_{trap} measured at low altitude by ELFIN B at L = 4.5 - 5.5 and 14–16 MLT increased and reached a high level near 4 UT on 6 March. The corresponding measured flux ratio J_{prec}/J_{trap} was also much larger at 4 UT on 6 March than before, following a 9-hr-long peak of $Kp \simeq 5$ indicative of strong injections (ELFIN data at MLT later than 14–16 or earlier than 4 is discarded due to statistically much lower chorus wave power at middle latitudes, see Agapitov et al., 2018, and Section 2).

In Figure 7a, the chorus wave power gain G is inferred, using Equation 6, from the variation of 180, 240, and 300 keV electron fluxes measured by ELFIN B at 14–16 MLT and L=4.5-5.5 during the 5–6 March 2022 storm, between the times indicated by vertical dashed green lines in Figure 6. Although Figure 7a contains much less data than Figure 5a, the best least squares fit $G\approx 2.9\cdot \left(J_{trap}(90^\circ)s^BL^4E/10^8\right)^{0.9986}$ shows a similar, linear scaling of the inferred chorus wave power gain G with the theoretical linear gain G_{th} . A second estimate of the relationship between the inferred wave power gain G and $G_{th} \simeq J_{trap}(90^\circ)s^BL^4E/\eta$ during this storm is provided in Figure 7b using only Equations 2–5. Figure 7b shows ΔG as a function of $\Delta(J_{trap}(90^\circ)s^BL^4E)$ and the best least

MOURENAS ET AL. 14 of 21



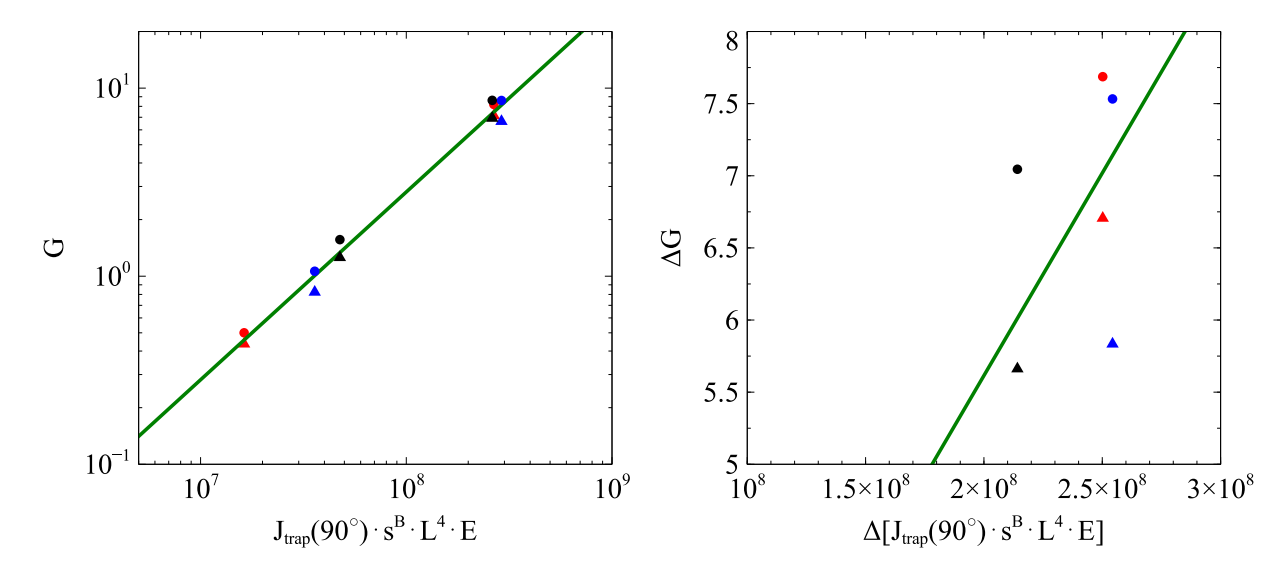


Figure 7. (a) Chorus wave power gains G as a function of J_{trap} (90°) s^BL^4E (with J_{trap} in e/cm²/s/sr/MeV and E in MeV) on 5–6 March 2022, inferred from low altitude 180 keV (bluck), 240 keV (blue), and 300 keV (red) electron flux measurements by ELFIN B at L=4.5-5.5 and 14–16 MLT. Such G values are inferred using J_{prec1} (circles) or J_{prec2} (triangles) during the time interval from 5 March (6 UT) to 6 March (3:40 UT) in Figure 6. The solid green line shows the best least squares power-law fit $G\approx 2.9\cdot \left(J_{trap}(90^\circ)s^BL^4E/10^8\right)^{0.9986}$. (b) ΔG as a function of $\Delta(J_{trap}(90^\circ)s^BL^4E)$ on 5–6 March 2022, with the best least squares linear fit $\Delta G=2.8\cdot \Delta(J_{trap}(90^\circ)s^BL^4E/10^8)$ with R=0.33 (green line).

squares linear fit, equivalent to $G = 2.8 \cdot (J_{trap} (90^{\circ}) s^B L^4 E/10^8)$, with a correlation coefficient R = 0.33. These results are again consistent with the Kennel-Petschek model.

4. Discussion of Results

The chorus wave power gains G(t) inferred in Section 3 usually reach \sim 3 times higher values at the time of maximum trapped \sim 100 - 300 keV electron fluxes during geomagnetic storms than the assumed maximum level $G_0 \simeq 3$ at the upper flux limit in the Kennel-Petschek model (Kennel & Petschek, 1966; Summers et al., 2009). This could simply correspond to short time intervals during which trapped fluxes could briefly exceed the Kennel-Petschek flux limit during a dynamical evolution toward an equilibrium state. However, the measured trapped \sim 80 - 500 keV electron fluxes were not particularly elevated during the 16–18 April 2021 event. They were rather consistent with, or somewhat lower than, the typical maximum trapped fluxes recorded for tens of hours around the end of such strong injections events (Hua, Bortnik, Chu, et al., 2022; Hua, Bortnik, & Ma, 2022; Mourenas, Artemyev, et al., 2022; Mourenas et al., 2023). The inferred gain G was also significantly higher than 3 from 17 to 18 April 2021. This suggests that the maximum inferred gains $G \approx 10$ probably correspond to the actual wave power gain G_0 at the upper flux limit.

Part of the discrepancy between the Kennel-Petschek estimates and observations probably stems from the presence of stronger nonlinear wave-particle interactions at higher trapped flux. The Kennel-Petschek model is based on quasi-linear diffusion theory, while numerical simulations and observations have demonstrated that nonlinear interactions can become significant for high wave amplitudes exceeding the threshold for electron trapping in the wave potential (Albert et al., 2013; Artemyev et al., 2016; Demekhov et al., 2017; Omura et al., 2007, 2008; Summers et al., 2011). However, in the presence of a typical population of chorus wave packets representative of statistical observations during active periods, consisting of mostly short and intense wave packets with random frequency and phase jumps (Mourenas, Zhang, et al., 2022; Zhang, Agapitov, et al., 2020; Zhang et al., 2021; Zhang, Mourenas, et al., 2020), the actual precipitation rates of 100–500 keV electrons can still be approximately described via the quasi-linear approach (Artemyev, Mourenas, et al., 2022; Gan et al., 2022; Mourenas et al., 2021; Mourenas, Zhang, et al., 2022; Zhang, Agapitov, et al., 2020), although nonlinear effects can lead to up to ~1.5 times faster electron diffusive-like pitch-angle transport, on average, at low equatorial pitch-angles than in pure quasi-linear diffusion (Artemyev, Mourenas, et al., 2022). A slightly faster increase of the total (quasi-linear and nonlinear) effective diffusion rate than the quasi-linear diffusion rate as wave amplitude

MOURENAS ET AL. 15 of 21

increases could therefore account for a $\sim 10\%$ to $\sim 20\%$ increase of the gain G inferred from Equation 6 at the highest J_{trap} compared to G inferred at the lowest J_{trap} .

It is worth emphasizing that in the proposed method, the inferred wave power gains depend, via Equation 2, on the ratio of pitch-angle diffusion rates $D_{\alpha\alpha}$ near the loss cone at two different times and also, in Equation 6, on the ratio of theoretical wave power gains G_{th} at these two different times. Therefore, the inferred gains G do not depend on the absolute level of $D_{\alpha\alpha}$ or G_{th} , but only on the relative variation of such quantities over time. This is a key advantage of this method. It means that the actual $D_{\alpha\alpha}$ and G_{th} do not need to be identical to the quasi-linear diffusion rate and to the linear convective gain, respectively, to obtain accurate estimates of G: the actual $D_{\alpha\alpha}$ and G_{th} only need to vary in time approximately proportionally to the quasi-linear $D_{\alpha\alpha}$ and to the linear G_{th} , respectively. In other words, nonlinear effects may increase the actual pitch-angle diffusion rates and wave power gains by constant factors compared to their quasi-linear and linear counterparts without affecting the accuracy of our G estimates. However, we caution that if the magnitude of such nonlinear amplification factors would significantly vary in time, then our G estimates could become biased.

The notion of a maximum gain value $G_0=3$ was introduced by Kennel and Petschek (1966) under the assumption that roughly $\sim 5\%$ of the generated whistler-mode waves could be reflected along field lines, yielding $G_0=\ln{(1/0.05)}=3$ to ensure a balance between wave generation and partial wave loss, allowing to maintain a quasi-equilibrium level of wave power. However, later studies have found that there is probably only a marginal reflection of $\lesssim 0.1\%$ of the average power of excited quasi-parallel chorus waves, which are usually strongly damped along their propagation to the high latitudes where partial reflection occurs (e.g., see Parrot et al., 2003; Chen et al., 2013; Agapitov et al., 2018; Meredith et al., 2020). Since this may partly correspond to wave reflection and propagation from other L-shells and/or other MLTs, such estimates of the reflection rate are probably valid only globally, over a substantial range of L-shells and MLTs. In the presence of such marginal wave reflection rates, reaching the high average amplitudes $B_w \sim 50\,\mathrm{pT}$ of chorus waves measured at low latitudes $\lambda \sim 10^\circ$ and 4–14 MLT during strong injections with $Kp \gtrsim 4$ (Agapitov et al., 2018; Meredith et al., 2020) would require wave power gains $G_0 > 7$ (as first noticed by Summers et al., 2009), consistent with our inferred wave power gains $G_0 > 10$ near the upper flux limit.

Besides, Van Allen Probes measurements during geomagnetic storms at $L \approx 5$ in 2013–2018 suggest the presence of an upper flux limit J_{trap} (90°) $\approx 5 \times 10^7$ e/cm²/s/sr/MeV at 180 keV (Hua, Bortnik, & Ma, 2022). This empirical upper limit may correspond to the Kennel-Petschek limit J_{KP} (90°) for $G_0 \sim 10$ and $s \sim 0.25$, if the total, linear and nonlinear wave power gain G is $\sim 15-30$ times larger than the linear gain G_{th} over a realistic distance $\Delta s \approx LR_E/10 - LR_E/5$. This is roughly compatible with the highest nonlinear to linear gain ratio obtained by Summers et al. (2011) at $L \approx 4$ for s = 0.3 and trapped electrons with a ~ 150 keV ring velocity distribution.

5. Conclusions

In this paper, we described a method, based on quasi-linear diffusion theory, allowing us to use low-altitude energy and pitch-angle resolved measurements of electron fluxes during geomagnetic storms leading to strong increases of trapped electron flux at $\sim 100-500$ keV, for inferring the wave-driven electron diffusion rate near the loss cone, the pitch-angle anisotropy of the electron population, the equatorial trapped electron flux and, finally, the wave power gain G(t) over the course of these events. An advantage of this method is that only low-altitude electron flux measurements are needed, provided that quasi-linear theory is applicable and average plasma parameters are weakly varying during each examined time interval (typically of the order of one day or less). This method allowed us to check whether two crucial assumptions of the Kennel-Petschek model, namely, the existence of a fixed maximum chorus wave power gain $G_0 \simeq 3$ near the upper flux limit and a linear increase of the wave power gain G with trapped flux J_{trap} , are justified in the Earth's outer radiation belt.

We showed that chorus wave power gains G(t) inferred from ELFIN CubeSat low-altitude measurements of $\sim 180-300$ keV electron fluxes steadily increase over the course of moderate geomagnetic storms at L=4.5-6.5. More importantly, we found that the inferred wave power gain G(t) is roughly proportional to the theoretical convective linear gain $G_{th} \sim J_{trap}$ (90°) s^BL^4E/η (Kennel & Petschek, 1966; Summers & Shi, 2014), as assumed in the Kennel-Petschek model, over a wide range of J_{trap} (90°) s^BL^4E , corresponding to a wide range of trapped electron flux.

MOURENAS ET AL. 16 of 21

Chorus wave power gains G(t) inferred from the selected low-altitude measurements of electron fluxes during geomagnetic storms regularly reach ~ 3 times higher values at the time of maximum trapped $\sim 100-300$ keV electron fluxes than their assumed level $G_0 \simeq 3$ at the upper flux limit in the Kennel-Petschek model (Kennel & Petschek, 1966; Summers et al., 2009). Since the measured trapped $\sim 80-500$ keV electron fluxes were consistent with, or slightly lower than, the typical maximum trapped fluxes recorded for tens of hours around the end of strong injection events (Hua, Bortnik, Chu, et al., 2022; Hua, Bortnik, & Ma, 2022; Mourenas, Artemyev, et al., 2022; Mourenas et al., 2023), and since the inferred gains G remained much higher than 3 from 17 to 18 April 2021, such maximum inferred gains $G \approx 10$ likely correspond to the actual chorus wave power gain G_0 at the upper flux limit. This would be equivalent to a ~ 3 times higher Kennel-Petschek flux limit than usually assumed (Kennel & Petschek, 1966; Mauk & Fox, 2010; Olifer et al., 2022; Summers et al., 2009; Summers & Shi, 2014).

The proposed method for inferring wave power gains is based, like the Kennel-Petschek model, on quasi-linear diffusion theory. Recent works have shown that the quasi-linear approach remains approximately correct in the presence of a typical population of mostly short and intense chorus wave packets during active periods, even when additional nonlinear effects at high wave amplitudes are taken into account (Artemyev, Mourenas, et al., 2022; Zhang, Agapitov, et al., 2020). Moreover, the inferred gain G depends on the ratio of two successive diffusion rates, and on the ratio of two successive theoretical wave power gains. Consequently, if actual diffusion rates, or theoretical wave power gains, are increased by some constant factors compared with quasi-linear or linear estimates, the accuracy of our inferred gains G should not be affected. The high inferred chorus wave power gains $G \approx 10$ near the upper flux limit have been attributed to the presence of a marginal high-latitude reflection rate of only $\approx 0.01 - 0.1\%$ of the power of quasi-parallel waves generated near the equator. Such a marginal wave reflection rate contrasts with the Kennel-Petschek assumption of a high reflection rate of $\approx 5\%$, but it is in better agreement with available observations and ray-tracing simulations in the presence of a strong Landau damping along wave propagation to high latitudes during disturbed periods (Agapitov et al., 2018; Chen et al., 2013; Meredith et al., 2020; Parrot et al., 2003).

Therefore, the present study provides empirical evidence in support of the Kennel-Petschek flux limit. Although a quasi-stable trapped electron flux requires a balance between the total number of electrons injected from the plasma sheet per second and the total number of electrons precipitated by the waves into the atmosphere per second near the upper flux limit (Etcheto et al., 1973; Mourenas et al., 2023) rather than merely a balance between wave generation and loss, the observed exponential increase of wave power with trapped flux and the high inferred wave power gain $G \approx 10$ near the upper flux limit corroborate the theoretical underpinnings of the Kennel-Petschek limit.

Notwithstanding, variations of wave Landau damping (Chen et al., 2013; Ke et al., 2021) and geomagnetic field configuration may modify the effective wave reflection rate and net power gain. This can probably lead to a variation of the maximum wave power gain G_0 at the upper flux limit by up to a factor of \sim 2 about its mean value $G_0 \approx 10$, in agreement with the observed variance of G for a fixed trapped flux in the present study. Finally, if wave-driven electron acceleration (Horne et al., 2005; Summers et al., 2002) becomes sufficiently strong to overcome wave-driven electron loss in a given energy range, the Kennel-Petschek flux limit, which explicitly assumes negligible energy diffusion and a net electron loss (Kennel & Petschek, 1966), may be replaced by another upper flux limit, corresponding to a dynamical equilibrium in the presence of electron injections and both pitch-angle and energy diffusion (Hua, Bortnik, & Ma, 2022; Mourenas, Artemyev, et al., 2022; Mourenas et al., 2023; Summers & Stone, 2022).

In their landmark study, Kennel and Petschek (1966) predicted the existence of an upper limit for trapped >100 keV proton fluxes, similar to the Kennel-Petschek limit for electrons, but due to a self-limitation through the generation of EMIC waves that efficiently scatter these protons into the atmosphere. Subsequently, Summers et al. (2017) used a relativistic reformulation of this limit in a cold multi-ion population and showed that proton fluxes measured at $L\approx 4$ during two geomagnetic storms approximately reached this limit. Accordingly, the present method could also be applied to infer EMIC wave power gains during strong ion injections in the dusk sector (Yahnin et al., 2021). This would similarly require energy and pitch-angle resolved measurements of trapped, precipitating, and backscattered proton fluxes, and sustained substorm ion injections leading to a progressive increase of proton flux and EMIC wave power, in the weak diffusion regime. As for chorus waves, a superposition of various intense EMIC waves may allow a diffusive-like proton transport toward the loss cone (Shoji & Omura, 2014).

MOURENAS ET AL. 17 of 21

21699402, 2024, 2, Downloaded

Data Availability Statement

ELFIN measurements are available at ELFIN Data Archive in CDF format (ELFIN, 2023). Dst, Sym - H, and Kp indices are available from the Kyoto World Data Center for Geomagnetism (WDC FOR GEOMAGNE-TISM, 2023). The SME index (Gjerloev, 2012) is available at the SuperMAG data archive (SUPERMAG, 2023).

Acknowledgments

A.V.A. and X.-J.Z. acknowledge support by NASA awards 80NSSC23K0403, 80NSSC22K0522, V.A. acknowledges ELFIN operations support from NASA NNX14AN68G and ELFIN science support from NSF AGS-1242918, AGS-2019950, and AGS-2329897. The authors are grateful to NASA's CubeSat Launch Initiative for ELFIN's successful launch in the desired orbits. They acknowledge early support of ELFIN project by the AFOSR, under its University Nanosat Program. UNP-8 project, contract FA9453-12-D-0285, and by the California Space Grant program. They acknowledge critical contributions of numerous volunteer ELFIN team student members.

References

- Agapitov, O. V., Mourenas, D., Artemyev, A., Breneman, A., Bonnell, J. W., Hospodarsky, G., & Wygant, J. (2021). Chorus and hiss scales in the inner magnetosphere: Statistics from high-resolution filter bank (FBK) van allen proves multi-point measurements. *Journal of Geophysical Research*, 126(7), e2020JA028998. https://doi.org/10.1029/2020JA028998
- Agapitov, O. V., Mourenas, D., Artemyev, A. V., Hospodarsky, G., & Bonnell, J. W. (2019). Time scales for electron quasi-linear diffusion by lower-band chorus waves: The effects of $\omega_{\rm pe}/_{\rm ce}$ dependence on geomagnetic activity. *Geophysical Research Letters*, 46(12), 6178–6187. https://doi.org/10.1029/2019GL083446
- Agapitov, O. V., Mourenas, D., Artemyev, A. V., Mozer, F. S., Hospodarsky, G., Bonnell, J., & Krasnoselskikh, V. (2018). Synthetic empirical chorus wave model from combined van allen Probes and cluster statistics. *Journal of Geophysical Research (Space Physics)*, 123(1), 297–314. https://doi.org/10.1002/2017JA024843
- Albert, J. M. (1993). Cyclotron resonance in an inhomogeneous magnetic field. *Physics of Fluids B*, 5(8), 2744–2750. https://doi.org/10.1063/1. 860715
- Albert, J. M. (2001). Comparison of pitch angle diffusion by turbulent and monochromatic whistler waves. *Journal of Geophysical Research*, 106(A5), 8477–8482. https://doi.org/10.1029/2000JA000304
- Albert, J. M., Tao, X., & Bortnik, J. (2013). Aspects of nonlinear wave-particle interactions. In D. Summers, I. U. Mann, D. N. Baker, & M. Schulz (Eds.), Dynamics of the earth's radiation belts and inner magnetosphere (pp. 255–264). https://doi.org/10.1029/2012GM001324
- Allanson, O., Watt, C. E. J., Ratcliffe, H., Allison, H. J., Meredith, N. P., Bentley, S. N., et al. (2020). Particle-in-Cell experiments examine electron diffusion by whistler-mode waves: 2. Quasi-linear and nonlinear dynamics. *Journal of Geophysical Research (Space Physics)*, 125(7), e27949. https://doi.org/10.1029/2020JA027949
- An, Z., Wu, Y., & Tao, X. (2022). Electron dynamics in a chorus wave field generated from particle-in-cell simulations. *Geophysical Research Letters*, 49(3), e2022GL097778. https://doi.org/10.1029/2022GL097778
- Angelopoulos, V., Tsai, E., Bingley, L., Shaffer, C., Turner, D. L., Runov, A., et al. (2020). The ELFIN mission. *Space Science Reviews*, 216(5), 103. https://doi.org/10.1007/s11214-020-00721-7
- Angelopoulos, V., Zhang, X. J., Artemyev, A. V., Mourenas, D., Tsai, E., Wilkins, C., et al. (2023). Energetic electron precipitation driven by electromagnetic ion cyclotron waves from ELFIN's low altitude perspective. *Space Science Reviews*, 219(5), 37. https://doi.org/10.1007/s11214-073-00984-w
- Artemyev, A. V., Agapitov, O., Mourenas, D., Krasnoselskikh, V., Shastun, V., & Mozer, F. (2016). Oblique whistler-mode waves in the Earth's inner magnetosphere: Energy distribution, origins, and role in radiation belt dynamics. *Space Science Reviews*, 200(1–4), 261–355. https://doi.org/10.1007/s11214-016-0252-5
- Artemyev, A. V., Mourenas, D., Zhang, X. J., & Vainchtein, D. (2022). On the incorporation of nonlinear resonant wave-particle interactions into radiation belt models. *Journal of Geophysical Research (Space Physics)*, 127(9), e30853. https://doi.org/10.1029/2022JA030853
- Artemyev, A. V., Zhang, X. J., Zou, Y., Mourenas, D., Angelopoulos, V., Vainchtein, D., et al. (2022). On the nature of intense sub-relativistic electron precipitation. *Journal of Geophysical Research (Space Physics)*, 127(6), e30571. https://doi.org/10.1029/2022JA030571
- Bell, T. F., Inan, U. S., Bortnik, J., & Scudder, J. D. (2002). The Landau damping of magnetospherically reflected whistlers within the plasmasphere. Geophysical Research Letters, 29(15), 1733. https://doi.org/10.1029/2002GL014752
- Birn, J., Thomsen, M. F., Borovsky, J. E., Reeves, G. D., McComas, D. J., Belian, R. D., & Hesse, M. (1998). Substorm electron injections: Geosynchronous observations and test particle simulations. *Journal of Geophysical Research*, 103(A5), 9235–9248. https://doi.org/10.1029/071A02635
- Bortnik, J., Thorne, R. M., Meredith, N. P., & Santolik, O. (2007). Ray tracing of penetrating chorus and its implications for the radiation belts. Geophysical Research Letters, 34(15), L15109. https://doi.org/10.1029/2007GL030040
- Boyd, A. J., Turner, D. L., Reeves, G. D., Spence, H. E., Baker, D. N., & Blake, J. B. (2018). What causes radiation belt enhancements: A survey of the van allen Probes era. *Geophysical Research Letters*, 45(11), 5253–5259. https://doi.org/10.1029/2018GL077699
- Chakraborty, S., Mann, I. R., Watt, C. E. J., Rae, I. J., Olifer, L., Ozeke, L. G., et al. (2022). Intense chorus waves are the cause of flux-limiting in the heart of the outer radiation belt. *Scientific Reports*, 12(1), 21717. https://doi.org/10.1038/s41598-022-26189-9
- Chen, L., Thorne, R. M., Li, W., & Bortnik, J. (2013). Modeling the wave normal distribution of chorus waves. *Journal of Geophysical Research*, 118(3), 1074–1088. https://doi.org/10.1029/2012JA018343
- Chen, L., Zhang, X.-J., Artemyev, A., Angelopoulos, V., Tsai, E., Wilkins, C., & Horne, R. B. (2022). Ducted chorus waves cause sub-relativistic and relativistic electron microbursts. *Geophysical Research Letters*, 49(5), e97559. https://doi.org/10.1029/2021GL097559
- Demekhov, A. G. (2011). Generation of VLF emissions with the increasing and decreasing frequency in the magnetosperic cyclotron maser in the backward wave oscillator regime. *Radiophysics and Quantum Electronics*, 53(11), 609–622. https://doi.org/10.1007/s11141-011-9256-x
- Demekhov, A. G., Nunn, D., & Trakhtengerts, V. Y. (2003). Backward wave oscillator regime of the whistler cyclotron instability in an inhomogeneous magnetic field. *Physics of Plasmas*, 10(11), 4472–4477. https://doi.org/10.1063/1.1620507
- Demekhov, A. G., Taubenschuss, U., & Santolík, O. (2017). Simulation of VLF chorus emissions in the magnetosphere and comparison with THEMIS spacecraft data. *Journal of Geophysical Research*, 122(1), 166–184. https://doi.org/10.1002/2016JA023057
- Demekhov, A. G., & Trakhtengerts, V. Y. (2008). Dynamics of the magnetospheric cyclotron ELF/VLF maser in the backward-wave-oscillator regime. II. The influence of the magnetic-field inhomogeneity. *Radiophysics and Quantum Electronics*, 51(11), 880–889. https://doi.org/10.1007/s11141-009-9093-3
- ELFIN. (2023). Electron Losses and fields investigation (ELFIN) data archive [Dataset]. Retrieved from https://data.elfin.ucla.edu/
- Etcheto, J., Gendrin, R., Solomon, J., & Roux, A. (1973). A self-consistent theory of plasmaspheric hiss. *Journal of Geophysical Research*, 78(34), 8150–8166. https://doi.org/10.1029/JA078i034p08150
- Gabrielse, C., Angelopoulos, V., Runov, A., & Turner, D. L. (2014). Statistical characteristics of particle injections throughout the equatorial magnetotail. *Journal of Geophysical Research*, 119(4), 2512–2535. https://doi.org/10.1002/2013JA019638

MOURENAS ET AL. 18 of 21

- Gan, L., Li, W., Ma, Q., Artemyev, A. V., & Albert, J. M. (2022). Dependence of nonlinear effects on whistler-mode wave bandwidth and amplitude: A perspective from diffusion coefficients. *Journal of Geophysical Research*, 127(5), e2021JA030063. https://doi.org/10.1029/2021JA030063
- Gjerloev, J. W. (2012). The SuperMAG data processing technique. Journal of Geophysical Research, 117(A9), A09213. https://doi.org/10.1029/ 2012JA017683
- Horne, R. B., Thorne, R. M., Glauert, S. A., Albert, J. M., Meredith, N. P., & Anderson, R. R. (2005). Timescale for radiation belt electron acceleration by whistler mode chorus waves. *Journal of Geophysical Research*, 110(A3), 3225. https://doi.org/10.1029/2004JA010811
- Hua, M., Bortnik, J., Chu, X., Aryan, H., & Ma, Q. (2022). Unraveling the critical geomagnetic conditions controlling the upper limit of electron fluxes in the Earth's outer radiation belt. *Geophysical Research Letters*, 49(22), e2022GL101096. https://doi.org/10.1029/2022GL101096
- Hua, M., Bortnik, J., & Ma, Q. (2022). Upper limit of outer radiation belt electron acceleration driven by whistler-mode chorus waves. Geophysical Research Letters, 49(15), e2022GL099618. https://doi.org/10.1029/2022GL099618
- Katoh, Y., & Omura, Y. (2016). Electron hybrid code simulation of whistler-mode chorus generation with real parameters in the Earth's inner magnetosphere. Earth Planets and Space, 68(1), 192. https://doi.org/10.1186/s40623-016-0568-0
- Katoh, Y., Omura, Y., Miyake, Y., Usui, H., & Nakashima, H. (2018). Dependence of generation of whistler mode chorus emissions on the temperature anisotropy and density of energetic electrons in the Earth's inner magnetosphere. *Journal of Geophysical Research*, 123(2), 1165–1177. https://doi.org/10.1002/2017JA024801
- Ke, Y., Chen, L., Gao, X., Lu, Q., Wang, X., Chen, R., et al. (2021). Whistler mode waves trapped by density irregularities in the Earth's magnetosphere. *Geophysical Research Letters*, 48(7), e92305. https://doi.org/10.1029/2020GL092305
- Kennel, C. F., & Petschek, H. E. (1966). Limit on stably trapped particle fluxes. Journal of Geophysical Research, 71, 1–28. https://doi.org/10.1029/jz071i001p00001
- Kuzichev, I. V., Soto-Chavez, A. R., Park, J., Gerrard, A., & Spitkovsky, A. (2019). Magnetospheric chorus wave simulation with the TRISTAN-MP PIC code. *Physics of Plasmas*, 26(7), 072901. https://doi.org/10.1063/1.5096537
- Li, W., & Hudson, M. K. (2019). Earth's van allen radiation belts: From discovery to the van allen Probes era. *Journal of Geophysical Research* (Space Physics), 124(11), 8319–8351. https://doi.org/10.1029/2018JA025940
- Li, W., Ni, B., Thorne, R. M., Bortnik, J., Green, J. C., Kletzing, C. A., et al. (2013). Constructing the global distribution of chorus wave intensity using measurements of electrons by the POES satellites and waves by the Van Allen Probes. *Geophysical Research Letters*, 40(17), 4526–4532. https://doi.org/10.1002/grl.50920
- Li, W., Santolik, O., Bortnik, J., Thorne, R. M., Kletzing, C. A., Kurth, W. S., & Hospodarsky, G. B. (2016). New chorus wave properties near the equator from Van Allen Probes wave observations. *Geophysical Research Letters*, 43(10), 4725–4735. https://doi.org/10.1002/2016GL068780
- Li, W., Thorne, R. M., Nishimura, Y., Bortnik, J., Angelopoulos, V., McFadden, J. P., et al. (2010). THEMIS analysis of observed equatorial electron distributions responsible for the chorus excitation. *Journal of Geophysical Research*, 115(A6), A00F11. https://doi.org/10.1029/20091A014845
- Li, X., Baker, D. N., Temerin, M., Reeves, G. D., & Belian, R. D. (1998). Simulation of dispersionless injections and drift echoes of energetic electrons associated with substorms. *Geophysical Research Letters*, 25(20), 3763–3766. https://doi.org/10.1029/1998GL900001
- Lyons, L. R., Thorne, R. M., & Kennel, C. F. (1971). Electron pitch-angle diffusion driven by oblique whistler-mode turbulence. *Journal of Plasma Physics*, 6(3), 589–606. https://doi.org/10.1017/S0022377800006310
- Mauk, B. H., & Fox, N. J. (2010). Electron radiation belts of the solar system. Journal of Geophysical Research, 115(A12), 12220. https://doi.org/10.1029/2010JA015660
- Meredith, N. P., Horne, R. B., Shen, X.-C., Li, W., & Bortnik, J. (2020). Global model of whistler mode chorus in the near-equatorial region (lλ_ml < 18°). *Geophysical Research Letters*, 47(11), e2020GL087311. https://doi.org/10.1029/2020GL087311
- Mourenas, D., Artemyev, A. V., Agapitov, O. V., & Krasnoselskikh, V. (2014). Consequences of geomagnetic activity on energization and loss of radiation belt electrons by oblique chorus waves. *Journal of Geophysical Research*, 119(4), 2775–2796. https://doi.org/10.1002/2013JA019674
- Mourenas, D., Artemyev, A. V., & Zhang, X.-J. (2019). Impact of significant time-integrated geomagnetic activity on 2-MeV electron flux. Journal of Geophysical Research: Space Physics, 124(6), 4445–4461. https://doi.org/10.1029/2019JA026659
- Mourenas, D., Artemyev, A. V., Zhang, X.-J., & Angelopoulos, V. (2022). Extreme energy spectra of relativistic electron flux in the outer radiation belt. *Journal of Geophysical Research: Space Physics*, 127(11), e2022JA031038. https://doi.org/10.1029/2022JA031038
- Mourenas, D., Artemyev, A. V., Zhang, X.-J., & Angelopoulos, V. (2023). Upper limit on outer radiation belt electron flux based on dynamical equilibrium. *Journal of Geophysical Research: Space Physics*, 128(8), e2023JA031676. https://doi.org/10.1029/2023JA031676
- Mourenas, D., Artemyev, A. V., Zhang, X.-J., Angelopoulos, V., Tsai, E., & Wilkins, C. (2021). Electron lifetimes and diffusion rates inferred from ELFIN measurements at low altitude: First results. *Journal of Geophysical Research: Space Physics*, 126(11), e2021JA029757. https://doi.org/10.1029/2021JA029757
- Mourenas, D., Zhang, X. J., Nunn, D., Artemyev, A. V., Angelopoulos, V., Tsai, E., & Wilkins, C. (2022). Short chorus wave packets: Generation within chorus elements, statistics, and consequences on energetic electron precipitation. *Journal of Geophysical Research (Space Physics)*, 127(5), e30310. https://doi.org/10.1029/2022JA030310
- Nogi, T., & Omura, Y. (2023). Upstream shift of generation region of whistler-mode rising-tone emissions in the magnetosphere. *Journal of Geophysical Research*, 128(3), e2022JA031024. https://doi.org/10.1029/2022JA031024
- Nunn, D., Santolik, O., Rycroft, M., & Trakhtengerts, V. (2009). On the numerical modelling of VLF chorus dynamical spectra. Annales Geophysicae, 27(6), 2341–2359. https://doi.org/10.5194/angeo-27-2341-2009
- O'Brien, T. P., & Moldwin, M. B. (2003). Empirical plasmapause models from magnetic indices. *Geophysical Research Letters*, 30(4), 1152. https://doi.org/10.1029/2002GL016007
- Olifer, L., Mann, I. R., Claudepierre, S. G., Baker, D. N., Spence, H. E., & Ozeke, L. G. (2022). A natural limit to the spectral hardness of worst case electron radiation in the terrestrial van allen belt. *Journal of Geophysical Research*, 127(8). e2022JA030506. https://doi.org/10.1029/2022JA030506
- Olifer, L., Mann, I. R., Kale, A., Mauk, B. H., Claudepierre, S. G., Baker, D. N., et al. (2021). A tale of two radiation belts: The energy-dependence of self-limiting electron space radiation. *Geophysical Research Letters*, 48(20), e2021GL095779. https://doi.org/10.1029/2021GL095779
- Omura, Y. (2021). Nonlinear wave growth theory of whistler-mode chorus and hiss emissions in the magnetosphere. *Earth Planets and Space*, 73(1), 95. https://doi.org/10.1186/s40623-021-01380-w
- Omura, Y., Furuya, N., & Summers, D. (2007). Relativistic turning acceleration of resonant electrons by coherent whistler mode waves in a dipole magnetic field. *Journal of Geophysical Research*, 112(A6), 6236. https://doi.org/10.1029/2006JA012243
- Omura, Y., Katoh, Y., & Summers, D. (2008). Theory and simulation of the generation of whistler-mode chorus. *Journal of Geophysical Research*, 113(A4), 4223. https://doi.org/10.1029/2007JA012622

MOURENAS ET AL. 19 of 21



Journal of Geophysical Research: Space Physics

- 10.1029/2023JA032193
- Omura, Y., & Nunn, D. (2011). Triggering process of whistler mode chorus emissions in the magnetosphere. *Journal of Geophysical Research*, 116(A5), A05205. https://doi.org/10.1029/2010JA016280
- Parrot, M., Santolík, O., Cornilleau-Wehrlin, N., Maksimovic, M., & Harvey, C. (2003). Magnetospherically reflected chorus waves revealed by ray tracing with CLUSTER data. Annales Geophysicae, 21(5), 1111–1120. https://doi.org/10.5194/angeo-21-1111-2003
- Press, W. H., Teukolsky, S. A., Vetterling, W. T., & Flannery, B. P. (2007). Numerical recipes: The art of scientific computing (3rd ed.). Cambridge University Press.
- Rosner, B. (1983). Percentage points for a generalized ESD many-outlier procedure. *Technometrics*, 25(2), 165–172. https://doi.org/10.1080/00401706.1983.10487848
- Schulz, M., & Davidson, G. T. (1988). Limiting energy spectrum of a saturated radiation belt. *Journal of Geophysical Research*, 93(A1), 59–76. https://doi.org/10.1029/JA093iA01p00059
- Shane, A. D., Marshall, R. A., Claudepierre, S. G., & Pettit, J. M. (2023). Electron lifetimes measured at LEO: Comparison with RBSP estimates and pitch angle resolved lifetimes. *Journal of Geophysical Research*, 128(8), e2023JA031679. https://doi.org/10.1029/2023JA031679
- Shapiro, V. D., & Sagdeev, R. Z. (1997). Nonlinear wave-particle interaction and conditions for the applicability of quasilinear theory. *Physics Reports*, 283(1–4), 49–71. https://doi.org/10.1016/S0370-1573(96)00053-1
- Sheeley, B. W., Moldwin, M. B., Rassoul, H. K., & Anderson, R. R. (2001). An empirical plasmasphere and trough density model: CRRES observations. *Journal of Geophysical Research*, 106(A11), 25631–25642. https://doi.org/10.1029/2000JA000286
- Shklyar, D. R. (1981). Stochastic motion of relativistic particles in the field of a monochromatic wave. Soviet Physics Journal of Experimental and Theoretical Physics, 53, 1192–1197.
- Shklyar, D. R., & Matsumoto, H. (2009). Oblique whistler-mode waves in the inhomogeneous magnetospheric plasma: Resonant interactions with energetic charged particles. Surveys in Geophysics, 30(2), 55–104. https://doi.org/10.1007/s10712-009-9061-7
- Shoji, M., & Omura, Y. (2014). Spectrum characteristics of electromagnetic ion cyclotron triggered emissions and associated energetic proton dynamics. *Journal of Geophysical Research*, 119(5), 3480–3489. https://doi.org/10.1002/2013JA019695
- Solovev, V. V., & Shkliar, D. R. (1986). Particle heating by a low-amplitude wave in an inhomogeneous magnetoplasma. Soviet Physics Journal of Experimental and Theoretical Physics, 63, 272–277.
- Summers, D., Ma, C., Meredith, N. P., Horne, R. B., Thorne, R. M., Heynderickx, D., & Anderson, R. R. (2002). Model of the energization of outer-zone electrons by whistler-mode chorus during the October 9, 1990 geomagnetic storm. *Geophysical Research Letters*, 29(24), 240000–240001. https://doi.org/10.1029/2002GL016039
- Summers, D., & Shi, R. (2014). Limiting energy spectrum of an electron radiation belt. *Journal of Geophysical Research*, 119(8), 6313–6326. https://doi.org/10.1002/2014JA020250
- Summers, D., Shi, R., Engebretson, M. J., Oksavik, K., Manweiler, J. W., & Mitchell, D. G. (2017). Energetic proton spectra measured by the van allen Probes. *Journal of Geophysical Research*, 122(10), 129–144. https://doi.org/10.1002/2017JA024484
- Summers, D., & Stone, S. (2022). Analysis of radiation belt killer electron energy spectra. *Journal of Geophysical Research*, 127(9), e2022JA030698. https://doi.org/10.1029/2022JA030698
- Summers, D., Tang, R., & Omura, Y. (2011). Effects of nonlinear wave growth on extreme radiation belt electron fluxes. *Journal of Geophysical Research*, 116(A10), 10226. https://doi.org/10.1029/2011JA016602
- Summers, D., Tang, R., Omura, Y., & Lee, D.-H. (2013). Parameter spaces for linear and nonlinear whistler-mode waves. *Physics of Plasmas*, 20(7), 072110. https://doi.org/10.1063/1.4816022
- Summers, D., Tang, R., & Thorne, R. M. (2009). Limit on stably trapped particle fluxes in planetary magnetospheres. *Journal of Geophysical Research*, 114(A10), 10210. https://doi.org/10.1029/2009JA014428
- Summers, D., Thorne, R. M., & Xiao, F. (1998). Relativistic theory of wave-particle resonant diffusion with application to electron acceleration in the magnetosphere. *Journal of Geophysical Research*, 103(A9), 20487–20500. https://doi.org/10.1029/98JA01740
- SUPERMAG. (2023). Geomagnetic indices at the SuperMag data archive [Dataset]. Retrieved from https://supermag.jhuapl.edu/indices/
- Tang, C. L., Wang, Y. X., Ni, B., Su, Z. P., Reeves, G. D., Zhang, J.-C., et al. (2017). The effects of magnetospheric processes on relativistic electron dynamics in the Earth's outer radiation belt. *Journal of Geophysical Research*, 122(10), 9952–9968. https://doi.org/10.1002/2017JA024407
- Tao, X., Bortnik, J., Albert, J. M., & Thorne, R. M. (2012). Comparison of bounce-averaged quasi-linear diffusion coefficients for parallel propagating whistler mode waves with test particle simulations. *Journal of Geophysical Research*, 117(A10), 10205. https://doi.org/10.1029/2012JA017931
- Tao, X., Thorne, R. M., Li, W., Ni, B., Meredith, N. P., & Horne, R. B. (2011). Evolution of electron pitch angle distributions following injection from the plasma sheet. *Journal of Geophysical Research*, 116(A4), A04229. https://doi.org/10.1029/2010JA016245
- Tao, X., Zonca, F., & Chen, L. (2017). Identify the nonlinear wave-particle interaction regime in rising tone chorus generation. Geophysical Research Letters, 44(8), 3441–3446. https://doi.org/10.1002/2017GL072624
- Tao, X., Zonca, F., Chen, L., & Wu, Y. (2020). Theoretical and numerical studies of chorus waves: A review. Science China Earth Sciences, 63(1), 78–92. https://doi.org/10.1007/s11430-019-9384-6
- Thorne, R. M., Li, W., Ni, B., Ma, Q., Bortnik, J., Chen, L., et al. (2013). Rapid local acceleration of relativistic radiation-belt electrons by magnetospheric chorus. *Nature*, 504(7480), 411–414. https://doi.org/10.1038/nature12889
- Trakhtengerts, V. Y., Demekhov, A. G., Titova, E. E., Kozelov, B. V., Santolik, O., Gurnett, D., & Parrot, M. (2004). Interpretation of Cluster data on chorus emissions using the backward wave oscillator model. *Physics of Plasmas*, 11(4), 1345–1351. https://doi.org/10.1063/1.1667495
- Tsai, E., Artemyev, A., Angelopoulos, V., & Zhang, X.-J. (2023). Investigating whistler-mode wave intensity along field lines using electron precipitation measurements. *Journal of Geophysical Research (Space Physics)*, 128(8), e2023JA031578. https://doi.org/10.1029/2023JA031578
- Tsurutani, B. T., & Smith, E. J. (1974). Postmidnight chorus: A substorm phenomenon. Journal of Geophysical Research, 79(1), 118–127. https://doi.org/10.1029/JA079i001p00118
- Turner, D. L., Angelopoulos, V., Li, W., Hartinger, M. D., Usanova, M., Mann, I. R., et al. (2013). On the storm-time evolution of relativistic electron phase space density in Earth's outer radiation belt. *Journal of Geophysical Research*, 118(5), 2196–2212. https://doi.org/10.1002/jgra. 50151
- Turner, D. L., Claudepierre, S. G., Fennell, J. F., O'Brien, T. P., Blake, J. B., Lemon, C., et al. (2015). Energetic electron injections deep into the inner magnetosphere associated with substorm activity. *Geophysical Research Letters*, 42(7), 2079–2087. https://doi.org/10.1002/
- WDC FOR GEOMAGNETISM. (2023). Geomagnetic indices at the WDC for geomagnetism. Kyoto, Japan [Dataset]. Retrieved from https://wdc.kugi.kyoto-u.ac.jp/wdc/Sec3.html

MOURENAS ET AL. 20 of 21



Journal of Geophysical Research: Space Physics

- 10.1029/2023JA032193
- Xiong, Y., Xie, L., Chen, L., Ni, B., Fu, S., & Pu, Z. (2018). The response of the energy content of the outer electron radiation belt to geomagnetic storms. *Journal of Geophysical Research*, 123(10), 8227–8240. https://doi.org/10.1029/2018JA025475
- Yahnin, A. G., Popova, T. A., Demekhov, A. G., Lubchich, A. A., Matsuoka, A., Asamura, K., et al. (2021). Evening side EMIC waves and related proton precipitation induced by a substorm. *Journal of Geophysical Research*, 126(7), e2020JA029091. https://doi.org/10.1029/2020JA029091
- Zhang, X. J., Agapitov, O., Artemyev, A. V., Mourenas, D., Angelopoulos, V., Kurth, W. S., et al. (2020). Phase decoherence within intense chorus wave packets constrains the efficiency of nonlinear resonant electron acceleration. *Geophysical Research Letters*, 47(20), e89807. https://doi.org/10.1029/2020GL089807
- Zhang, X.-J., Angelopoulos, V., Mourenas, D., Artemyev, A., Tsai, E., & Wilkins, C. (2022). Characteristics of electron microburst precipitation based on high-resolution ELFIN measurements. *Journal of Geophysical Research (Space Physics)*, 127(5), e30509. https://doi.org/10.1029/20221A030509
- Zhang, X. J., Demekhov, A. G., Katoh, Y., Nunn, D., Tao, X., Mourenas, D., et al. (2021). Fine structure of chorus wave packets: Comparison between observations and wave generation models. *Journal of Geophysical Research (Space Physics)*, 126(8), e29330. https://doi.org/10.1029/2021JA029330
- Zhang, X. J., Mourenas, D., Artemyev, A. V., Angelopoulos, V., Bortnik, J., Thorne, R. M., et al. (2019). Nonlinear electron interaction with intense chorus waves: Statistics of occurrence rates. *Geophysical Research Letters*, 46(13), 7182–7190. https://doi.org/10.1029/2019GL083833
- Zhang, X. J., Mourenas, D., Artemyev, A. V., Angelopoulos, V., Kurth, W. S., Kletzing, C. A., & Hospodarsky, G. B. (2020). Rapid frequency variations within intense chorus wave packets. *Geophysical Research Letters*, 47(15), e88853. https://doi.org/10.1029/2020GL088853

MOURENAS ET AL. 21 of 21